R. & M. No. 3479

R. & M. No. 3479

MINISTRY OF TECHNOLOGY

AERONAUTICAL RESEARCH COUNCIL
REPORTS AND MEMORANDA

Temperature and Pressure Studies in the Reservoir of a Reflected-Shock Hypersonic Tunnel

By K. C. LAPWORTH and J. E. G. TOWNSEND

LONDON: HER MAJESTY'S STATIONERY OFFICE
1967
PRICE 18*s.* 6*d.* NET

Temperature and Pressure Studies in the Reservoir of a Reflected-Shock Hypersonic Tunnel

By K. C. LAPWORTH and J. E. G. TOWNSEND

Reports and Memoranda No. 3479*
December, 1964

Summary.

Temperatures and pressures have been measured in the shock-heated gas upstream of the nozzle of a reflected-shock hypersonic tunnel. Temperatures were measured by spectrum-line reversal, using sodium *D* lines for some measurements and the blue resonance lines of chromium for others. The temperature and pressure measurements immediately behind the first reflected-shock wave agreed well with theory but subsequent variations in temperature and pressure did not agree very well with theory. These differences between theory and experiment are attributed to boundary-layer development and contact region behaviour. In particular, the duration of the shock-heated gas at the higher shock Mach numbers was much less than theory predicts and much less than pressure measurements alone indicated. This appears to be due to encroachment of the contact region into the shock-heated gas at the closed end of the tube, and presents a limitation to the running time of a shock tunnel at high enthalpies.

LIST OF CONTENTS

*Replaces N.P.L. Aero Report 1127—A.R.C. 26 110.

Section

1. *Introduction.*

The reflected-shock tunnel has been used for some years now for the generation of short duration, high enthalpy, hypersonic flow[1,2,3]. This paper gives an account of the pressure and temperature development with time in the region of the reflecting end of a hypersonic shock tunnel, using nitrogen as the test gas and helium as the driver gas. A helium-nitrogen combination 'tailors'* at an incident shock Mach number of 3·4, giving a reflected-shock temperature of 1574°K when the initial gas temperature is 20°C. Since interest has centred on temperatures above this tailoring temperature, most of the work described in this report was carried out at above-tailoring conditions. Ideal theory of the shock tube (*see* Appendix IV) indicates that, at above-tailoring conditions, a shock wave is reflected off the contact face and this wave is then multiply-reflected between the end of the tube and the contact surface. According to ideal theory, this wave becomes very weak after a few reflections, resulting in constant properties of the hot gas. This prediction is not confirmed by the present measurements. Even in the tailored case, when there are no secondary reflections, the measurements do not indicate rapid attainment of constant properties predicted by theory. Boundary-layer effects appear to be important in modifying the temperature and pressure histories but these effects are not fully understood at present.

*The 'tailored' condition is that condition under which no disturbance is reflected off the contact surface when the reflected shock meets it (*see* Ref. 1).

At the higher values of incident shock Mach number, it is observed that the duration of high temperature is much less than ideal theory predicts. This observation has been made in earlier work, using hydrogen as the driver gas[4,5,6]. This early fall in temperature is attributed to mixing at the contact face between the cold driver gas and the shock-heated test gas. The mixing may be brought about by instability of the contact face under the impulsive acceleration due to the reflected-shock wave. It is this rapid cooling of the shock-heated gas at the higher enthalpies that represents the true running-time of a reflected-shock hypersonic tunnel. This is much shorter than pressure measurements alone indicate, since pressure is constant across the contact surface and the mixing would not be evident from pressure measurements alone.

2. *The Shock Tunnel.*

The shock tunnel consists of a shock tube with one end closed except for a small orifice leading to an expansion nozzle to generate hypersonic flow. The orifice was blanked off for the present series of experiments so that the apparatus was used as a shock tube. This tube has a driver section 14 ft long, driven section 18 ft long and internal diameter of 3 in. Helium was used as driver gas which was separated from the nitrogen test gas by an aluminium diaphragm. The diaphragms used for this work were 0·079 in. thick and had a centrally-placed milled cross 0·025 in. deep. The bursting pressure was 430 p.s.i. $\pm$ 10 p.s.i. The incident shock speed was determined near the reflecting end of the tube by three platinum resistance films at distances of 0·5 in., 16·25 in. and 28·25 in. from the closed end. Microsecond counters were used to determine the shock speed between consecutive resistance films. Small windows for temperature measurement were fitted 0·5 in. away from the blanked-off end of the tube. The windows were cemented in brass holders which could be easily removed for cleaning or replacement. It was found necessary to renew the windows after about 50 runs because of pitting of the glass surfaces. A few temperature measurements were also made 2·5 in. away from the end of the shock tube by inserting a make-up piece between the end of the tube and the section containing the windows.

Pressure measurements were made at a distance of 0·5 in. from the end of the tube. A pressure measuring point was also provided at a distance of 15·75 in. from the end of the tube so that the pressure gauge could be calibrated dynamically using the incident shock wave.

3. *Method of Temperature Measurement.*

The principle of the method has been described in detail in Ref. 7 and only a brief description will be given here.

The hot gas whose temperature is to be determined is seeded with a suitable material which gives rise to a strong spectrum line and this line is viewed against the continuum of a high temperature, incandescent background source, usually a tungsten filament lamp, if the temperature to be measured is below 2900°K. Then, provided that the area of the image of the source and the solid angle accepted are the same for the hot gas and the background source, the spectrum line will be seen in emission or absorption against the background continuum according as the gas temperature is greater or less than the brightness temperature of the backing source. If the brightness temperature is adjusted until the spectrum line disappears against the continuum, then the gas temperature is equal to this brightness temperature.

In applying this method to the shock tube, sodium, in the form of a smoke of sodium chloride, or chromium, in the form of chromium carbonyl vapour, is mixed with the test gas (nitrogen). When the gas is heated by passage of the shock wave, free sodium or free chromium atoms are formed by decomposition of the sodium chloride or chromium carbonyl. The spectrum lines used for reversal temperature measurements are the resonance D lines in the case of sodium and the resonance blue lines in the case of chromium.

A photomultiplier is set on the reversal lines, which are isolated from the remainder of the spectrum by a monochromator or optical interference filter and the signal from the photomultiplier is displayed on an oscilloscope. The photomultiplier then indicates emission or absorption according as the gas temperature is greater or less than the background brightness temperature; when there is no change in

signal, then the background brightness temperature is equal to the gas temperature. The lamp brightness temperature is determined with a disappearing filament pyrometer. In practice, the shock tube has to be fired several times, re-adjusting the backing temperature between each firing so as to approach the match condition. It proves very difficult to achieve an exact match since the gas temperature is very sensitive to shock wave speed and this cannot be reproduced accurately from run to run. Therefore, it is usually only known whether the gas temperature is greater or less than the brightness temperature of the backing source. This method has, however, led to useful results in studying the reservoir conditions in a reflected-shock tunnel[4,5].

The actual gas temperature can, however, be determined if a double-beam system is used similar in principle to that used by Clouston, Gaydon and Hurle[8(a)]. This method relies on using two separate single beam systems with one backing source temperature deliberately set higher than the expected gas temperature and the other backing source set at a lower temperature than the expected gas temperature. Thus, one photomultiplier shows an emission signal and the other shows an absorption signal. If it is now assumed that the concentration of reversal atoms is the same for each beam then the relative displacements of the two oscilloscope traces are a measure of the difference in temperature between the backing sources and the gas temperature. If the temperature difference between the two backing sources is not too great and each optical system and photomultiplier is set to have the same sensitivity, then linear interpolation using the two signals is sufficient to determine the gas temperature. The double-beam system is considered in detail in Appendix I. The double-beam system has now been adopted in the work described in this report. Two forms have been used: in the first arrangement two beams mutually perpendicular were used and in the second arrangement two beams following paths close to each other were used (Figs. 1 and 2). The latter system has proved more convenient for temperature measurements in the hypersonic shock tunnel. A general view of this system is shown in Plate 1. This system has the advantage that, if the concentration of reversal atoms is not uniform, it will be affected less than the former system in which the beams follow very different paths.

When sodium was used for reversal temperature measurements, it was initially introduced into the nitrogen as a smoke of sodium chloride obtained by heating a little salt on a coil mounted in the shock tube. This gave very little control over the amount of sodium chloride introduced or the uniformity of dispersal of the smoke. This system was later replaced by another in which nitrogen was led over salt heated above its melting point in a vitreosil tube contained in a tubular furnace. The temperature of the furnace was maintained at 850°C at which temperature molten salt has a vapour pressure of 0·8 mm Hg. A smoke of sodium chloride was produced in the nitrogen: this was passed through two settling bottles to remove large solid particles and then led into the shock tube. The wavelength region corresponding to the yellow sodium D lines was isolated from the remainder of the spectrum by means of an optical interference filter of bandwidth 70Å and peak transmission 74 per cent. E.M.I. 6094C photomultipliers were used to measure the emission and absorption signals.

When chromium was used for reversal temperature measurements, a mixture of nitrogen and chromium carbonyl vapour was prepared by leaving nitrogen in contact with solid chromium carbonyl in a 25 litre flask. The vapour pressure of chromium carbonyl is about 0·1 mm of mercury at room temperature[23] (20°C). Thus, known mixtures of nitrogen and chromium carbonyl could be prepared. The blue resonance lines of chromium at 4290Å, 4275Å and 4254Å were used for reversal temperature measurements. In initial work, the wavelength region corresponding to these three blue lines was isolated by a monochromator. In later work the monochromator was replaced by a narrow band optical interference filter of bandwidth 30Å and peak transmission 47 per cent. Chromium was more convenient to use than sodium because of the ease with which the chromium carbonyl can be mixed with the nitrogen. However, because the blue resonance lines are of higher energy than the yellow sodium resonance lines, successful temperature measurements could not be made below about 2000°K. Sodium, however, could be used down to about 1400°K.

The background sources initially used were 'Pointolite' lamps in which a small tungsten bead is heated to incandescence by a small electric arc struck on it. This source, however, suffers from the disadvantage that the small tungsten bead changes its position when the temperature of the lamp is altered.

This movement is due to the bead being supported on a bimetallic strip which automatically moves the bead from the striking position to the running position. The small additional movements brought about by change of brightness temperature often makes realignment of the optical system necessary. Another possible disadvantage of the 'Pointolite' is that the emissivity of tungsten has been measured in the form of flat strip only and this may differ from the emissivity of tungsten in the form of a small bead, as in the 'Pointolite' source.

The background sources finally used were microscope illuminators having a flat tungsten filament as shown in Plate 2. Each end of the filament is bent back and attached to a support so that, when the filament is viewed directly, the ends of the filament which are cooled by conduction to the filament supports are not seen. It was found from optical pyrometer measurements that the brightness temperature of the part of the filament viewed directly does not vary by more than about 10°K along the middle third of its length.

The signal from each photomultiplier was displayed on a double-beam oscilloscope (Tektronix 502) and photographed with an oscilloscope camera fitted with a Polaroid-Land back. In order to obtain temperatures from the traces, the results were treated as shown in Appendix I. In this way the variation of temperature with time was deduced.

Both backing sources are imaged in the shock tube and it is necessary to know the brightness temperature of these images at the wavelength of the reversal line. Corrections must be made for reflections at the surfaces of the windows and lenses between the backing sources and the centre of the shock tube, and also for the variation of the emissivity of tungsten with temperature and wavelength. These corrections are dealt with in detail in Appendix II.

The brightness temperature of a lamp filament was determined using a Leeds and Northrup disappearing filament pyrometer which measures the brightness temperature at 6650Å. This pyrometer was checked regularly against a secondary standard lamp that has been calibrated at the National Physical Laboratory. The brightness temperature, measured by the pyrometer, was calibrated against the voltage developed across a low resistance in series with each lamp, measured with a digital voltmeter. The brightness temperature of each lamp can be quickly adjusted and measured, using this calibration. The calibration was checked at intervals and was found to be constant for a given lamp.

Each backing source required direct currents up to 20 Amps. Each source was therefore provided with its own supply consisting of 4 12-volt car batteries connected in parallel and the current was controlled by a variable ballast resistor.

Care had to be taken in setting up the optical system to ensure that the apertures and field slits were properly filled. In order to check that the optical arrangement was correct, a number of trial temperature measurements at approximately the same shock Mach number were made with increasing aperture size for each measurement. For apertures less than a critical size, the temperature measurements were independent of aperture diameter; above this critical size measured temperature increased rapidly with the aperture diameter. Care was taken to ensure that temperature measurements were always made with the aperture smaller than the critical value.

The accuracy of the temperature measurements depends on the signal-to-noise ratio of the signals from the photomultipliers[7]. The signal-to-noise ratio could be improved at the expense of response time. The time constant of the associated circuitry was somewhat less than 6 microseconds, which was adequate for the time-scale of the phenomena investigated.

4. *Experimental Results.*

4.1. *Temperature Measurements.*

Temperatures measured behind the shock wave initially reflected off the closed end of the shock tube were found to agree quite well with theoretical values given by Bernstein[9] as can be seen in Fig. 3 (*see* Fig. 26 for notation). It was estimated that temperatures could be measured with an accuracy of ± 30°K. The measured speed of the incident shock wave could be in error by 1 per cent at the higher shock Mach numbers: a 1 per cent error in M_s at $M_s = 4{\cdot}5$ is equivalent to 40°K error in temperature, i.e., 0·14 error

in T_{A3}/T_{A1}. Thus, the total error in T_{A3}/T_{A1} could amount to $\pm 0{\cdot}24$. Therefore, the experimental points shown in Fig. 3 agree with Bernstein's theory, within the limits of experimental error. Temperature histories at a distance of 0·5 in. from the end plate were obtained from oscillograms similar to that shown in Fig. 4. Results are presented for shock Mach numbers ranging from 3·20* to 4·75 in Figs. 5 to 9. A temperature history for shock Mach number 4·41 at a distance of 2·5 in. from the closed end of the tube is presented in Fig. 10. The experimental points in these figures are compared with the theoretical temperature predictions derived from theoretical wave diagrams. Two such wave diagrams, one for the lowest shock Mach number 3·20 and one for the highest shock Mach number 4·75, are shown in Figs. 11 and 12. The computation of the wave interactions in a shock tube is dealt with in Appendix IV.

The details of the development of temperature with time are reserved for the discussion in Section 5.

4.2. *Relative Concentration of Reversal Atoms.*

The relative concentration of reversal atoms may be determined as described in Appendix I. Results for $M_s = 3{\cdot}39$ and $M_s = 4{\cdot}45$ are given respectively in Figs. 13 and 14. The full curves show the relative concentration of reversal atoms as deduced from the double-beam oscillograms used for temperature determination. The dotted curves give the relative density in the gas as deduced from the separate measurements of temperature and pressure. The full and the dotted curves have been adjusted to coincide at small values of the time. For a given mass of reversal atoms introduced into the gas, the full and the dotted curves should, ideally, coincide until the temperature begins to fall. The large discrepancies between the measured relative concentration of reversal atoms and the deduced relative density of the gas are discussed more fully below in Section 5.

4.3. *Pressure Measurements.*

The pressure was measured at a distance of 0·5 in. from the reflecting end of the shock tube. An S.L.M. PZ14 gauge was used in conjunction with an S.L.M. PV17 electrometer amplifier for the pressure measurements. It was found that static calibration of the gauge gave a response about 20 per cent lower than dynamic calibration: the reasons for this are not at present known. Since the gauge was used to measure the sudden change in pressure behind the reflected shock wave, the dynamic calibration was employed. This was obtained by placing the gauge in the shock tube at a distance of 15·75 in. from the closed end and observing the response to the pressure step behind incident shock waves. It was found that a mechanical 'ringing' signal of about 40 kilocycles per sec was produced in the gauge when the shock tube was fired. This ringing was removed by connecting between the output of the electrometer amplifier and the oscilloscope a 'double-T' filter designed to reject the 40 kilocycles per sec signal.

Oscilloscope traces showing the reflected shock pressure and the later development of pressure with time are shown in Fig. 15. From such traces, used in conjunction with the dynamic calibration, the value of p_{A3}/p_{A1} was obtained where p_{A3} is the pressure behind the first shock wave reflected from the closed end and p_{A1} is the pressure initially in the low pressure section of the tube. The measured pressures immediately behind the reflected shock wave are compared with real gas theory in Fig. 16. The estimated accuracy of the pressure measurements is ± 5 per cent. The changes of pressure with time are shown in Figs. 5–9 where the shock Mach numbers are close to those for which temperature measurements were obtained.

4.4. *Comparison between the Duration of High Pressure and the Duration of Luminous Radiation from Excited Reversal Atoms.*

The temperature and pressure measurements presented above were not made simultaneously but they indicate that, at the higher incident shock Mach numbers, the duration of high temperature becomes much less than the duration of high pressure. In order to investigate this further, experiments were performed in which the gas pressure and the light from the reversal atoms were recorded simultaneously

---

*The results for $M_s = 3{\cdot}20$ are near the lower limit of temperature measurement and therefore are not as accurate as the temperature measurements at higher values of M_s.

At this low value of M_s, the difference in the two background temperatures was 320°K which was too high for determination of the temperature by linear interpolation of the photomultiplier signals. The exact relationship of equation I(12), Appendix I, was used for evaluation of the temperature.

on a dual-beam oscilloscope. The observations were made 0·5 in. from the reflecting end of the tube. Three traces, obtained at incident shock Mach numbers of 3·66, 3·96 and 4·52, are shown in Figs. 17–19. The radiation signal depends on the concentration and the temperature of the reversal atoms. For an optically thick spectrum line, the total radiation in the line is proportional to $N^{\frac{1}{2}} e^{-\frac{h\nu}{kT}}$, where N is the concentration of reversal atoms, ν the frequency of the reversal line and the remaining symbols have their usual meaning. Thus, the radiation has a weak dependence on particle concentration but is strongly dependent on temperature. In order to obtain a very approximate measure of the duration of high temperature, it is assumed that the radiation is a function of temperature only. The duration of high temperature is then taken to be the duration for which the radiation is more than 10 per cent of its maximum value. Using sodium line reversal in the range 1400°K–2000°K, this implies that the duration of high temperature is that time for which the temperature is within approximately 85 per cent of its maximum value. The same criterion holds for the chromium resonance blue lines in the temperature range 2000°K–3000°K.

The duration of high pressure is taken to be the time between shock reflection and the advent of the reflected head of the expansion wave.

The duration of high temperature and the duration of high pressure are shown plotted on the same graph as a function of incident shock Mach number in Fig. 20.

5. *Discussion.*

5.1. *Temperature and Pressure just Behind the Reflected Shock Wave.*

The temperature and pressure just behind the reflected shock wave and 0·5 in. away from the end plate are seen to be in good agreement with the theoretical results of real gas theory for pure nitrogen given by Bernstein[9] (Fig. 3). In these experiments, however, the nitrogen contained small amounts of chromium carbonyl or sodium chloride. Heat is required to dissociate these compounds and, in the case of sodium chloride, heat is also required to evaporate the solid particles. This leads to a lowering of the temperature. The effect of various concentrations of these additives on the gas properties behind the incident and reflected-shock waves in nitrogen has been examined theoretically by Schofield[10]. Using the results of Ref. 10, chromium carbonyl, in molecular concentrations of a few tenths of 1 per cent, lowers the temperature in the range 2000°K to 3000°K by roughly 10°K per 0·1 per cent concentration. The chromium carbonyl concentration in these experiments ranged from 0·1 per cent at $M_s = 4{\cdot}00$ to 0·3 per cent at $M_s = 4{\cdot}9$. The scatter of the results shown on Fig. 3 is, however, greater than these expected systematic depressions of the temperature and it is concluded that random errors mask any lowering of temperature due to chromium carbonyl addition. The concentration of sodium chloride in the nitrogen was not so easily determined and only a very rough estimate was obtained by weighing the tube containing the sodium chloride before and after passing nitrogen over the heated salt. From this it was estimated that the molecular concentration of sodium chloride suspended in the gas was of the order 0·05 per cent. According to Ref. 10, this would lead to a temperature drop of less than 10°K even if all the sodium chloride were decomposed. This is small compared with the scatter of the results.

5.2. *Initial Development of the Temperature and Pressure.*

The pressure behind the reflected shock wave initially rises for all incident shock strengths. The duration of this initial rise is 0·7 ms at the lowest incident shock Mach number of 3·2 but decreases to 0·3 ms at the highest shock Mach number of 4·75. This rise in pressure behind the reflected shock wave has been attributed by Rudinger to a pressure gradient along the tube behind the incident shock wave, associated with the development of the boundary layer and the consequent attenuation of the incident shock wave[11]. This pressure gradient is magnified by the reflected shock wave, giving rise to the observed increase of pressure with time at the end plate. The attenuating incident shock wave is also associated with a temperature gradient along the tube, as observed by Holbeche and Spence, for example[12]; this would be expected to lead to an observed increase in temperature with time behind the reflected shock wave, in phase with the observed pressure rise. If the observed pressure rise of the gas near the end plate is due to an isentropic compression, then the associated temperature rise would be 40°K at the lowest incident shock Mach numbers, $M_s = 3{\cdot}2$, and 100°K at the highest Mach number, $M_s = 4{\cdot}75$. However, a rise in temperature corresponding to the initial rise in pressure is not observed.

The apparent failure of the temperature to follow the initial pressure rise is probably due to boundary-layer effects. The boundary layer, being cooler and denser than the core of the gas, will lead to absorption of radiation which will be interpreted as a lowering of the measured temperature. The lowering of the measured temperature due to these effects has been treated theoretically for the case of a laminar boundary layer[31] but the turbulent boundary layer has not been considered. In addition to the increased concentration of reversal atoms in the boundary layer associated with the increased density, the concentration, and consequently the self-absorption is probably further increased by removal from the walls of compounds of the reversal atom deposited in previous runs. This would account for the observed rapid initial increase in reversal atom concentration noted above (Section 4.2, Figs. 13 and 14). The concentration of reversal atoms continues to rise after the passage of the reflected shock wave: this is consistent with gas motion in the region behind the reflected shock wave removing material from the wall. This interesting conclusion is considered in more detail below (Section 5.5). The phenomenon appears to be too complex to make an estimate of the lowering of the measured temperature due to this effect. The initial increase in temperature associated with the pressure increase and the lowering of the measured temperature due to self-absorption at the boundary tend to cancel each other; Figs. 6–9 show a fairly steady temperature or slightly falling temperature for the first few hundred microseconds. (The temperature results at the lowest shock Mach number of 3·2, Fig. 5, are inconclusive because of the scatter of the measurements at this low temperature).

The initial rise in pressure is followed by a small fall and, corresponding to this fall, a small temperature fall is also observed in Figs. 6–9. Such a fall in pressure has been qualitatively accounted for by Woods when the reflected shock interacts with a laminar boundary layer[13]. According to Ref. 13, the pressure fall is due to accumulation of boundary-layer fluid at the junction between the shock and the wall when the boundary layer does not have sufficient energy to negotiate the pressure rise across the reflected-shock wave. This phenomenon has been observed by Mark[14] and has also been treated theoretically by Byron and Rott[15]. However, under the conditions of the present experiments, the reflected-shock wave almost certainly interacts, for the most part, with a turbulent boundary layer. The transition to turbulence behind the incident shock wave is discussed in Appendix III. From the conclusions of this appendix, it was possible to prepare the curves of Fig. 21, showing the distance from the end plate and the time after reflection at which the reflected-shock wave is likely first to encounter a turbulent boundary layer. These curves are only tentative but they do show that the reflected-shock wave is likely to meet a turbulent boundary layer very soon after reflection.

Although the dip in pressure and temperature can be explained in the case of interaction between the reflected shock wave and a laminar boundary layer, it is not quite clear at present whether the same conclusion may be extended to the case of a turbulent boundary layer. This needs further investigation before any definite conclusion is made. Similar pressure results have been observed and discussed by Davies and Edwards[16].

5.3. *Interaction of the Reflected Shock Wave with the Contact Region.*

The dip in pressure and temperature is followed by a rise in these quantities over the whole Mach number range, from below tailoring to above tailoring. In Figs. 5 to 9, it is seen that this rise in pressure and temperature occurs considerably earlier than the first disturbance off the contact surface given by ideal theory. The ideal contact surface position, which neglects boundary-layer effects, is shown, for example, in the wave diagrams of Figs. 11 and 12. However, due to boundary-layer development, the real contact surface will be closer to the shock wave than shown on the ideal wave diagrams, giving rise to an earlier appearance of the disturbance reflected off the contact surface after interaction with the reflected shock wave. Using Mirels' theory[17] of shock tube test time limitation due to a turbulent boundary layer, it has been possible to calculate the time of arrival at the end of the shock tube of the disturbance reflected off the real contact surface. The results, showing ideal theory, Mirels' theory and experimental results, are shown in Fig. 22 and it is seen that the experimental points lie quite close to Mirels' theory.

One outstanding difficulty is that a compression is always initially observed reflected from the contact face, even for the undertailored case as in Fig. 5. However, some mixing probably takes place between the driver and test gas when the diaphragm opens, due to finite opening time of the diaphragm, as suggested, for example, in Ref. 18. Initially then, the reflected shock wave may meet a mixture of driver and driven gas under conditions that could conceivably give rise to a reflected compression wave, although the overall conditions may be undertailored. The non-uniform contact region has been treated theoretically by Chisnell[19] and more recently by Bird[20]. Chisnell has shown that the final strength of the wave reflected from a contact region is the same as would be obtained if the shock wave were reflected from a contact surface; therefore, using this result, an expansion wave should follow a compression wave initially reflected off the contact region for the undertailored case, which, in fact, is observed (Fig. 5). In the overtailored cases, the compression reflected from the contact region is seen to rise rather slowly contrasting with the ideal sharp rise given by a shock wave: this, in fact, is what would be expected in reflection of a shock wave from a contact region rather than a contact surface. In particular, the tailored case of Fig. 6 is of interest since, contrary to ideal theory, the pressure and temperature do not remain unchanged after the reflected shock has interacted with the contact region but rise and fall as a compression and expansion wave are reflected off the contact region.

5.4. *Final Development of Temperature and Pressure.*

In the below-tailoring result, Fig. 5, the temperature falls with the pressure as the expansion wave is reflected from the contact region. The temperature falls to a value too low to be measured by the line-reversal technique. The pressure does not fall to the ideal theoretical value but drops to a value somewhat above this and then rises uniformly with time. Ideal theory indicates that the multiple wave reflections between the closed end of the tube and the contact surface rapidly become very weak, as shown on the idealised wave diagram of Fig. 11, leading to a steady pressure. This final rise in pressure, actually observed before the advent of the reflected head of the expansion wave, has been mentioned briefly in Ref. 21, where it is noted that the rate of pressure increase becomes greater as the incident shock Mach number increases. At the higher incident shock Mach number of Ref. 21, part of the pressure rise can be accounted for by the early appearance of the tail of the expansion wave associated with the burst diaphragm. Over Mach number range of the present experiments, however, the tail of the expansion wave should always reach the closed end of the driven section later than the head of the expansion wave reflected from the closed end of the driver section.

The most likely cause of the observed final pressure increase would appear to lie in the presence of non-uniform pressures along the tube, associated with development of the boundary layer, and is similar to the pressure increase observed very soon after shock reflection (Section 5.2). This rise in pressure is observed over the whole Mach number range but cannot be shown on Figs. 7 to 9 because of their expanded time scales.

The temperature shows very different behaviour from the pressure. Figs. 5 and 6 show results below tailoring and at tailoring. After the wave has been reflected off the contact region, the temperature falls although the pressure is rising. In Figs. 7 to 9, showing results above tailoring, the pressure level attained after the compression off the contact region agrees well with theory but the temperature fails to attain the theoretical level. The difference between the measured temperature and the temperature given by ideal theory increases with increasing incident shock strength. Not only does the temperature fail to reach the theoretical value, but it falls away rapidly, this fall becoming more marked as the shock Mach number is increased. This fall in temperature, particularly at the higher shock strengths, presents a serious limitation to the hot running time when the facility is used as a shock tunnel.

The results for reversal atom concentration given in Figs. 13 and 14 indicate a dependence of concentration on temperature after the initial rise. This is reasonable in the case of sodium (Fig. 13) for, under the conditions corresponding to this record, the dissociation of sodium chloride is sensitive to the temperature (*see* Ref. 10). The apparent dependence of chromium atom concentration on temperature is more difficult to understand since, according to Wilkerson, at the temperatures corresponding

to Fig. 14, all the chromium carbonyl may be expected to be completely dissociated (*see* Appendix B of Ref. 23). Wilkerson suggests the dissociation reaction:

$$Cr(CO)_6 \rightleftharpoons Cr + 6CO.$$

However, the reaction may well be more complicated than this. Gaydon and Hurle have demonstrated spectroscopically that chromium oxide is formed behind a shock wave in nitrogen containing chromium carbonyl[8(b)]. Chromium oxide is a refractory compound and may well exhibit a temperature dependent dissociation at the temperatures corresponding to Fig. 14. The way in which chromium oxide is formed is not understood at present.

Fig. 10 shows the temperature history for $M_s = 4{\cdot}41$ at a distance of 2·5 in. from the closed end of the driven section. The initial dip and subsequent rise in temperature are present as in the other traces but they are separated by a shorter time interval, because the measuring station is closer to the contact region. From Mirels' theory[17], the disturbance from the contact region should appear 0·3 ms after the reflected shock passes the measuring station. Experiment, however, indicates that this disturbance appears 0·1 ms after the reflected shock (Fig. 10). This difference of 0·2 ms between Mirels' theory and experiment is consistent with Fig. 22 where some of the results show a difference of as much as 0·2 ms.

The later fall and rise of Fig. 10 are difficult to understand. There is a final fall of temperature, as observed in the measurements made close to the end of the tube, but the fall occurs earlier in this case since the observation is made closer to the contact region.

5.5. *The Cooling of the Shock-Heated Gas.*

The duration of high temperature in the shock-heated nitrogen is much less at the higher shock strengths than ideal theory indicates. This limitation becomes quite severe as shock strength increases as indicated by the oscillograms of Figs. 17–19 and the curve shown in Fig. 20.

The possible mechanisms leading to heat loss are: (a) conduction to the cold walls of the tube, (b) convection losses to the cooled walls, (c) radiation losses and (d) actual mixing between the cold driver gas and the shock-heated nitrogen. The possibility of heat loss by conduction alone has been examined using Goldsworthy's theory[22] and the loss was found to be negligible during the short duration of high temperature. Again, radiation losses prove to be negligible. Heat loss by convection is, however, difficult to assess. Theoretically, in the one-dimensional flow, free of boundary layers, the hot gas is brought to rest behind the reflected-shock wave. Experiments show, however, that this idealised theoretical model differs considerably from the real situation. There is evidence of gas motion behind the reflected-shock wave. Wilkerson, for example, has detected residual motion towards the end wall with a velocity of about 3 per cent or 4 per cent of the reflected-shock speed[23]. Schlieren photographs in Ref. 24 also show the presence of vortices moving across the end plate toward the centre of the plate. Mark's more refined theory[14], which takes account of the influence of a laminar boundary layer on reflected-shock speed, also indicates that there will be residual gas motion toward the end plate. Such motion would lead to forced convective heat transfer but it is difficult at present to make an estimate of the magnitude of such losses.

Mixing of the cold driver gas with the shock-heated gas seems to be a possible cause of temperature fall. One mechanism that has been suggested to account for this mixing is Taylor instability of the contact region under the impulsive action of the reflected-shock wave (*see*, for example, Ref. 25). Taylor treated the problem of the stability of an interface between two incompressible fluids under steady acceleration and showed that the interface is unstable when the acceleration is directed from the less dense to the more dense fluid[26]. The present problem, however, is concerned with the stability of an interface between two *compressible* fluids under the action of an *impulsive* change in velocity. The case of an impulsive acceleration imposed on an interface between two *incompressible* fluids has been examined by Stuart[27] and also by Markstein[28]. Their treatment, which neglects viscosity and compressibility, indicates that instability results regardless of the direction of acceleration. Richtmyer has treated numerically the case of impulsive acceleration of the interface between two compressible fluids in the

direction from less dense to more dense fluid[29]. The fluids were assumed to have the same value of γ and the same initial temperature. The computations, which were carried out for initial density ratios across the interface of 0·125 and 0·0625 showed that the interface was unstable. One interesting result shown by Richtmyer for these cases, is that the ultimate growth of corrugations of the interface agree with incompressible theory to within 5 per cent to 10 per cent, suggesting that compressibility effects may well be small.

The theory of Markstein has been applied to the contact region stability problem by Bird, Martin and Bell and they found that, by making a suitable assumption about the shape of the interface, they were able to obtain quite good agreement between evaluated results of testing time using this theory and measured results[30].

Taking the origin of the x co-ordinate at the contact surface, Markestein's theory gives the disturbance velocity, u', by the following expression:

$$u' = \delta u \, kA \left(\frac{\rho_{B2} - \rho_{A2}}{\rho_{B2} + \rho_{A2}} \right)$$

where

δu = change in velocity of the contact surface induced by the shock wave

$k = \dfrac{2\pi}{\lambda}$

λ = wavelength of the contact surface shape

A = initial amplitude of the wave

ρ_{B2}, ρ_{A2} = densities on either side of the contact surface (*see* Fig. 26 for notation).

The reflected-shock wave is moving in the positive x-direction. From studies on the contact surface it is known that this interface is convex towards the closed end of the driven tube which means that kA is negative (*see*, for example, Ref. 24). u is positive. Therefore, when $\rho_{B2} > \rho_{A2}$, the disturbance velocity, u', is negative; i.e., the disturbance velocity of the interface is directed towards the closed end of the tube. Theoretically, this condition is met when $M_s > 3{\cdot}58$. On the other hand, when $M_s < 3{\cdot}58$, then $\rho_{B2} < \rho_{A2}$ and the disturbance velocity of the interface is directed away from the reflecting end of the driven tube. $M_s = 3{\cdot}58$ implies neutral stability, resulting in zero disturbance velocity. Thus, discounting the effect of the reflected head of the expansion wave from the driver section, and discounting heat losses other than contact surface mixing due to instability, the high temperature duration would, according to Markstein's theory, become infinite at an incident shock Mach number of 3·58. The experimental high temperature duration curve in Fig. 20 increases steeply at roughly $M_s = 3{\cdot}8$. At the lower Mach numbers, the duration is limited by the reflected expansion wave from the driver section rather than by contact surface instability. It is felt that there is at least a qualitative agreement between infinite duration at $M_s = 3{\cdot}58$ predicted using Markstein's theory and the observed trend of the duration curve.

At the higher incident shock Mach numbers, the fall off in radiation is very definite as seen, for example, in the result for $M_s = 4{\cdot}52$, Fig. 19. At the lower values of M_s, however, the fall in observed radiation is far less well defined as seen in the result for $M_s = 3{\cdot}66$, Fig. 17. Mixing between hot and cold gas at the contact surface is probably not a dominant cooling mechanism at the lower incident shock Mach numbers: however, there is a slow fall in radiation before the appearance of the reflected expansion wave, indicating that there is some cooling. It is suggested that other cooling mechanisms may account for this slow fall. In particular, forced convective cooling may be important but it is difficult to evaluate this at present.

6. *Conclusions and Suggestions for Further Work.*

Pressures and temperatures measured near the end plate of the shock tube agree well with theory immediately after reflection. The pressure, however, initially increases with time, due to an axial pressure gradient associated with boundary-layer growth and consequent shock attenuation. The measured temperature is not observed to increase in harmony with this pressure increase. It appears likely that the temperature measurements are lowered by increased concentration of reversal atoms in the cooler boundary layer. This increased concentration is attributed to the increase in density in the boundary layer and also to removal of reversal atom compounds from the shock tube walls.

This initial pressure rise is followed by a dip and temperature records show a small fall in harmony with this. This small fall in pressure and temperature is not fully understood at present but it is thought to be associated with interaction between the reflected-shock wave and a turbulent boundary layer. Accumulation at the shock-wall junction of boundary fluid of insufficient energy to negotiate the reflected-shock wave could lead to the observed fall in pressure and temperature.

This fall is followed by a second rise in both pressure and temperature. This compression is identified as the disturbance reflected off the contact region when it meets the reflected-shock wave. It is observed that this initial disturbance off the contact region is always a compression even at under-tailored conditions. This is tentatively attributed to the gradation of properties through the contact region which could, even in the under-tailored case, give rise to an initial compression followed by an expansion, when struck by the reflected-shock wave. This, in fact, is what is observed in the under-tailored case. After the fall in pressure and temperature in this case, the pressure then rises slowly but the temperature continues to fall.

At conditions above tailoring, the rise in pressure and temperature associated with the compression off the contact region is followed by a continued rise in pressure but a fall in temperature. The rise in pressure is attributed to boundary-layer development along the whole tube. The fall in temperature becomes very rapid at incident shock Mach numbers above 3·8 and represents a marked decrease in the available running time of a reflected-shock tunnel at high temperatures. This rapid fall in temperature at the higher incident shock Mach numbers is attributed largely to mixing between the hot, shock-heated nitrogen and the much cooler helium at the contact region. This mixing be may due to instability of the contact region under the impulsive action of the reflected-shock wave. A calculation based on incompressible stability theory shows qualitative agreement with the observations.

At incident shock Mach numbers below 3·8 the temperature fall is less drastic. The slower fall, observed before the appearance of the head of the expansion wave reflected from the end of the driver section, is probably due largely to forced convective heat transfer.

The gas properties in the region between the end plate and the reflected-shock wave are not very constant in time, even for tailored-interface conditions, and this should be borne in mind when using this region as a reservoir for a hypersonic shock tunnel, or for physical-chemical experiments on gases behind reflected-shock waves.

Some of the above conclusions are tentative and the following problems are suggested for further study:

(1) The effect of initial pressure level in the tube on the temperature and pressure behaviour in the reflected-shock region should be investigated. In the present experiments, a constant bursting pressure was used and the initial pressure of nitrogen was rather low in order to attain the higher shock Mach numbers. (At $M_s = 4{\cdot}75$ the value of the initial pressure was 45 mm Hg.) At a given value of M_s, the boundary-layer thickness will be affected by the pressure level and, in fact, the thinner boundary layers obtained at the higher pressures used in much of the shock-tunnel research may be an advantage.

(2) The interaction of a reflected-shock wave in a shock tube with a turbulent wall boundary layer should be investigated theoretically and experimentally.

(3) A theoretical study should be made of the interaction between a shock wave and various models of the contact region to investigate the nature of the disturbance reflected off the region when struck by the reflected-shock wave.

(4) The problem of the stability of a contact region between two compressible fluids under the impulsive acceleration due to a shock wave should be investigated.

(5) Cooling by forced convection in the reflected-shock region should be examined experimentally.

Acknowledgements.

Miss S. Henney helped with the experiments. The authors are particularly grateful to Dr. L. Davies for numerous invaluable discussions during the preparation of this report and for help and advice during the pressure measurements. Helpful discussions with Dr. D. Schofield and Dr. J. T. Stuart are also gratefully acknowledged. Dr. E. W. E. Rogers and Dr. L. Pennelegion read the manuscript and made helpful criticisms.

REFERENCES

No.	Author(s)	Title, etc.
1	C. E. Wittliff, M. R. Wilson and A. Hertzberg	The tailored-interface hypersonic shock tunnel. *Journal of the Aeronautical Sciences*, Vol. 26, pp. 219–228. 1959.
2	A. Hertzberg, C. E. Wittliff and J. G. Hall	Development of the shock tunnel and its application to hypersonic flight. '*Hypersonic Flow Research*'. Academic Press, New York, 1962.
3	D. W. Holder and D. L. Schultz	On the use of shock tunnels for research on hypersonic flow. *Proceedings of Second International Congress in the Aeronautical Sciences*, Zurich, 1960. Vol. 3, pp. 59–86.
4	K. C. Lapworth, J. E. G. Townsend and K. Bridgeman	Reservoir temperature measurements in a hypersonic shock tunnel by sodium line reversal. Part I. Single beam method. A.R.C. 23 341. December, 1961.
5	K. C. Lapworth	Temperature measurements in a hypersonic shock tunnel. AGARDograph 68: '*The high temperature aspects of hypersonic flow*' pp. 255–269. Pergamon Press, 1964.
6	A. Q. Eschenroeder, J. W. Daiber, T. C. Golian and A. Hertzberg	Shock tunnel studies of high-enthalpy ionized airflows. AGARDograph 68: '*The high temperature aspects of hypersonic flow*' pp. 217–254.Pergamon Press, 1964.
7	K. C. Lapworth	Spectrum line reversal techniques of temperature measurements. Proceedings of the Symposium on *Some Developments in Techniques for Temperature Measurement*, April, 1962. pp. 29–37. Published by The Institution of Mechanical Engineers, London, 1963.
8(a)	J. G. Clouston, A. G. Gaydon and I. R. Hurle	Temperature measurements of shock waves by spectrum-line reversal. II. A double-beam method. *Proc. Roy. Soc.* A, Vol. 252, pp. 143–155. 1959.
8(b)	A. G. Gaydon and I. R. Hurle	Temperature measurements of shock waves and detonations by spectrum-line reversal. III. Observations with chromium lines. *Proc. Roy. Soc.* A, Vol. 262, p. 38. 1961.
9	L. Bernstein	Tabulated solutions of the equilibrium gas properties behind the incident and reflected normal shock-wave in a shock-tube. I. Nitrogen. II. Oxygen. A.R.C. C.P.626. April, 1961.
10	D. Schofield	Shock properties for nitrogen containing additives. A.R.C. 26 111.
11	G. Rudinger	Effect of boundary-layer growth in a shock tube on shock reflection from a closed end. *The Physics of Fluids*, Vol. 4, 1961. pp. 1463–1473.
12	T. A. Holbeche and D. A. Spence	A theoretical and experimental investigation of temperature variation behind attenuating shock waves. *Proc. Roy. Soc.*, A., Vol. 279, pp. 111–128. 1964.
13	B. A. Woods	A linearized investigation of the effect of a wall boundary layer on the motion of a reflected shock. A.R.C. 24 571. October, 1962.

No.	*Author(s)*	*Title, etc.*
14	Herman Mark	The interaction of a reflected shock wave with the boundary layer in a shock tube. NACA TM.1418. March, 1958.
15	S. Byron and N. Rott ..	On the interaction of the reflected shock wave with the laminar boundary layer on the shock tube walls. *Proceedings of the* 1961 *Heat Transfer and Fluid Mechanics Institute.* Stanford University Press, 1961.
16	L. Davies and D. H. Edwards	An experimental investigation of the reflected-shock pressure-time profiles for air, oxygen, nitrogen, argon, carbon dioxide and acetylene. A.R.C. R & M 3446. November, 1964.
17	H. Mirels	Shock tube test time limitation due to turbulent-wall boundary layer. *AIAA Journal*, Vol. 2, January, 1964. pp. 84–93.
18	D. R. White	Influence of diaphragm opening time on shock-tube flows. *Journal of Fluid Mechanics*, Vol. 4, 1958. pp. 585–599.
19	R. F. Chisnell	The normal motion of a shock wave through a non-uniform one-dimensional medium. *Proc. Roy. Soc.* A, Vol. 232, pp. 350–370. November, 1955.
20	G. A. Bird	The motion of a shock wave through a region of non-uniform density. *Journal of Fluid Mechanics*, Vol. 11, 1961. pp. 180–186.
21	D. W. Holder and D. L. Schultz	On the flow in a reflected-shock tunnel. A.R.C. R & M 3265. August, 1960.
22	F. A. Goldsworthy	The structure of a contact region, with application to the reflection of a shock from a heat-conducting wall. *Journal of Fluid Mechanics*, Vol. 5, 1959. pp. 164–176.
23	T. Wilkerson	The use of the shock tube as a spectroscopic source with an application to the measurement of *gf*-values for lines of neutral and singly ionized chromium. The University of Michigan Technical Note 02822–3–T. June, 1961.
24	D. W. Holder, C. M. Stuart and R. J. North	The interaction of a reflected shock with the contact surface and boundary layer in a shock tube. A.R.C. 22 891. September, 1961.
25	—	Agardograph 68: *The High Temperature Aspects of Hypersonic Flow* Discussion, p. 771. Pergamon Press. 1964.
26	G. I. Taylor	The instability of liquid surfaces when accelerated in a direction perpendicular to their planes. *Proc. Roy. Soc.* A, Vol. 201, pp. 192–196. 1950.

No.	*Author(s)*	*Title, etc.*
27	J. T. Stuart	Private Communication.
28	G. H. Markstein	Flow disturbances induced near a slightly wavy contact surface, or flame front, traversed by a shock wave. *Journal of Aeronautical Sciences*, Vol. 24, 1957. p. 238.
29	R. D. Richtmyer ..	Taylor instability in shock acceleration of compressible fluids. *Communications on Pure and Applied Mathematics*, Vol. XIII, 297–319. 1960.
30	K. D. Bird, J. F. Martin ..	Recent developments in the use of the hypersonic shock tunnel as a research and development facility. Third Hypervelocity Techniques Symposium, Denver. March, 1964. *Proceedings of Third Symposium on Hypervelocity Techniques*, University of Denver. March 1964.
31	K. C. Lapworth	Effect of laminar boundary layer development in a shock tube on spectrum-line reversal temperature measurements. A.R.C. 24 615. March, 1963.
32	Mitchell and Zemansky ..	*Resonance radiation and excited atoms.* C.U.P. 1961.
33	J. C. De Vos	A new determination of the emissivity of tungsten ribbon. *Physica XX*, 690–714. 1954.
34	R. D. Larrabee	Res. Lab. of Electronics, M.I.T. Tech. Rept. No. 328. May, 1957.
35	R. A. Hartunian, A. L. Russo and P. V. Marrone	Boundary-layer transition and heat transfer in shock tubes. *Journal of the Aerospace Sciences*, Vol. 27, 1960. No. 8, pp. 587–594.
36	D. Bitondo, I. I. Glass and G. N. Patterson ..	One-dimensional theory of absorption and amplification of a plane shock wave by a gaseous layer. UTIA Rept. No. 5. June, 1950.
37	I. J. Billington and I. I. Glass	On the one-dimensional refraction of a rarefaction wave at a contact surface. UTIA Rept. No. 31. April, 1955.
38	J. Hilsenrath, et al	*Tables of thermodynamic and transport properties of air, argon, carbon dioxide, carbon monoxide, hydrogen, nitrogen, oxygen and steam.* Pergamon Press, 1960.

APPENDIX I

Relationship between the Photomultiplier Signals, Temperature and Reversal Atom Concentration in a Double-Beam System

Consider the arrangement shown in Fig. 23. The backing source of brightness temperature T_B is focused into the shock tube and this image is, in turn, focused on to the slit in front of a photomultiplier. The light from the backing source completely fills the aperture stop and the slit. The total light flux incident on the photomultiplier is proportional to area of slit × solid angle of light entering the slit, i.e. proportional to $\omega_3 A_3$. Referring to Fig. 23, by Gaussian optics,

$$\omega_1 A_1 = \omega_2 A_2 = \omega_3 A_3. \qquad \text{I(1)}$$

Before the arrival of the shock wave, the photomultiplier 'sees' only the backing source. The flux of light, F_1, entering the photomultiplier is given by

$$F_1 = \omega_1 A_1 \int_{\Delta\nu_2} \xi_\nu B(\nu, T_B) d\nu \qquad \text{I(2)}$$

where ξ_ν is the transmission coefficient of the interference filter, $\Delta\nu_2$ the bandwidth of the filter and $B(\nu, T_B)$ the Planck radiation function.

When the gas is heated by the passage of the shock wave through it, free reversal atoms are formed by decomposition of the sodium chloride or chromium carbonyl and these atoms interact with the radiation from the backing source. The flux of light, F_2, that now enters the photomultiplier comprises that light which penetrates through the gas from the backing source together with the light emitted by the hot gas. In Ref. 31 it is shown that

$$F_2 = \omega_1 A_1 \int_{\Delta\nu_2} \xi_\nu B(\nu, T_B) \exp\left\{ -\int_{-R}^{+R} \alpha_\nu(x) dx \right\} d\nu +$$

$$+ \frac{\omega_1 A_1}{4\pi} \int_{\Delta\nu_1} \xi_\nu \int_{-R}^{+R} \varepsilon_\nu(x) \exp\left\{ -\int_{x}^{R} \alpha_\nu(x') dx' \right\} dx\, d\nu \qquad \text{I(3)}$$

where α_ν is the absorption coefficient per unit length and ε_ν is the emission coefficient per unit volume. These quantities are here regarded as functions of x, the radial distance from the centre of the shock tube. R is the radius of the shock tube. $\Delta\nu_1$ is the bandwidth of the reversal line. In thermodynamic equilibrium,

$$\varepsilon_\nu = 4\pi\alpha_\nu B(\nu, T). \qquad \text{I(4)}$$

The bandwidth of the filter, $\Delta\nu_2$ is greater than the bandwidth of the spectrum line $\Delta\nu_1$. Outside the range $\Delta\nu_1$ α_ν becomes 0 and therefore the first integral in I(3) can be given by

$$\int_{\Delta\nu_2} \xi_\nu B(\nu,T_B) \exp\left\{-\int_{-R}^{+R} \alpha_\nu(x)dx\right\} d\nu = \int_{\Delta\nu_1} \xi_\nu B(\nu,T_B) \exp\left\{-\int_{-R}^{+R} \alpha_\nu(x)dx\right\} d\nu +$$

$$+\int_{\nu_0-\frac{1}{2}\Delta\nu_2}^{\nu_0-\frac{1}{2}\Delta\nu_1} \xi_\nu B(\nu,T_B)d\nu + \int_{\nu_0+\frac{1}{2}\Delta\nu_1}^{\nu_0+\frac{1}{2}\Delta\nu_2} \xi_\nu B(\nu,T_B)d\nu. \qquad \text{I(5)}$$

The last two integrals of I(5) contribute only to unwanted 'noise' and should be made as small as possible by making the bandwidth of the filter only just wide enough to pass the reversal line. If I_n denotes the sum of these two 'noise' integrals, then using I(4) and I(5), I(3) becomes

$$F_2 = \omega_1 A_1 \int_{\Delta\nu_1} \xi_\nu B(\nu,T_B) \exp\left\{-\int_{-R}^{+R} \alpha_\nu(x)dx\right\} d\nu +$$

$$+\omega_1 A_1 \int_{\Delta\nu_1} \xi_\nu \int_{-R}^{+R} \alpha_\nu(x)\, B(\nu,T) \exp\left\{-\int_{x}^{R} \alpha_\nu(x')dx'\right\} dx\, d\nu +$$

$$+\omega_1 A_1 I_n \qquad \text{I(6)}$$

where T, the gas temperature and α_ν, the absorptivity are functions of x.

Similarly, the flux F_1 may be written

$$F_1 = \omega_1 A_1 \int_{\Delta\nu_1} \xi_\nu B(\nu,T_B)\, d\nu + \omega_1 A_1 I_n. \qquad \text{I(7)}$$

The change in light flux incident on the photomultiplier when the shock passes causes a change in output signal which is recorded as a deflection, d, on an oscilloscope trace. If the response of the photomultiplier varies linearly with light flux, then

$$d \propto F_2 - F_1$$

and, using I(6) and I(7), we may write

$$d = G \int_{\Delta\nu_1} \xi_\nu \left\{\int_{-R}^{+R} \alpha_\nu(x)\, B(\nu,T) \exp\left[-\int_{x}^{R} \alpha_\nu(x')dx'\right] dx -\right.$$

$$\left. -B(\nu,T_B)\left[1-\exp\left(-\int_{-R}^{+R} \alpha_\nu(x)dx\right)\right]\right\} d\nu \qquad \text{I(8)}$$

where G is a constant depending on ωA and photomultiplier sensitivity. Equation I(8) relates the observed deflection of an oscilloscope trace to the temperature, $T(x)$, and the absorptivity $\alpha_\nu(x)$ throughout the gas for a quite general distribution of temperature and absorptivity. The actual temperature, T, of the hot gas may only be found if some simplifying assumptions are made regarding the forms of the functions $T(x)$ and $\alpha_\nu(x)$. The simplest assumption to make is that the temperature, $T(x)$, is constant across the gas. Noting that

$$\int_{-R}^{+R} \alpha_\nu(x)\, B(\nu,T) \exp\left\{-\int_{x}^{R} \alpha_\nu(x')dx'\right\} dx =$$

$$= B(\nu,T)\left[\exp\left\{-\int_{x}^{R} \alpha_\nu(x')dx'\right\}\right]_{-R}^{+R}$$

$$= B(\nu,T)\left[1-\exp\left\{-\int_{-R}^{+R} \alpha_\nu(x)dx\right\}\right],$$

equation I(8) becomes

$$d = G\int_{\Delta\nu_1} \xi_\nu \left[1-\exp\left\{-\int_{-R}^{+R} \alpha_\nu(x)dx\right\}\right]\left[B(\nu,T)-B(\nu,T_B)\right]d\nu. \qquad \text{I(9)}$$

This leads to the important result that if $d>0$ (i.e., the signal is in emission relative to the backing source) then $T>T_B$. On the other hand, if $d<0$ (i.e., the signal is in absorption, then $T<T_B$). If $d=0$, then the gas temperature is equal to the brightness temperature of the backing source at the wavelength of the reversal line. The Planck function changes very little over the bandwidth of a reversal spectrum line and may be taken to be constant. Equation I(9) may then be written

$$d = G[B(\nu_0,T)-B(\nu_0,T_B)]\phi \qquad \text{I(10)}$$

$$\phi = \int_{\Delta\nu_1} \xi_\nu \left[1-\exp\left\{-\int_{-R}^{+R} \alpha_\nu(x)dx\right\}\right] d\nu.$$

If now a double-beam system is used in which the stops in each beam are adjusted so that the response of each photomultiplier is the same when the backing brightness temperatures are the same, then the deflections d_1 and d_2 resulting when the backing temperatures are T_1 and T_2 and the gas temperature T are given by

$$\begin{aligned} d_1 &= G[B(\nu_0,T)-B(\nu_0,T_{B1})]\phi \\ d_2 &= G[B(\nu_0,T_{B2})-B(\nu_0,T)]\phi \end{aligned} \qquad \text{I(11)}$$

where it is assumed that $T_{B2}>T>T_{B1}$, d_1 is the strength of the signal in emission and d_2 is the strength absorption. It is also assumed that ϕ is the same for each beam. This is reasonable since the distribution of reversal atoms throughout the gas is likely to be uniform.

From equations I(11), it is readiiy shown that

$$B(\nu_0,T) = B(\nu_0,T_{B1}) + \frac{d_1}{d_1+d_2}\left[B(\nu_0,T_{B2}) - B(\nu_0,T_{B1})\right]. \qquad \text{I(12)}$$

This is not a very convenient expression for obtaining the temperature and the reduction of the oscillograms to temperature is very much simplified if the following approximations are made:

(1) The Planck black-body function is replaced by Wien's approximation, which is a good approximation at optical frequencies and at the temperatures of interest here. That is,

$$B(\nu_0,T) = \frac{2h\nu_0^3}{c^2} e^{-\frac{h\nu_0}{kT}}$$

Using this approximation in I(11), it may be shown that

$$T = T_{B1} + (T_{B2} - T_{B1})\frac{d_1}{d_1+\beta d_2} \qquad \text{I(13)}$$

where

$$\beta = \frac{T_{B2}-T}{T-T_{B1}} \cdot \frac{1-\exp\left\{-\frac{h\nu_0}{k}\left(\frac{1}{T_{B1}}-\frac{1}{T}\right)\right\}}{\exp\left\{\frac{h\nu_0}{k}\left(\frac{1}{T}-\frac{1}{T_{B2}}\right)\right\}-1}. \qquad \text{I(14)}$$

(2) The approximation $\beta = 1$ is now made and I(13) reduces to

$$T = T_{B1} + (T_{B2} - T_{B1})\frac{d_1}{d_1+d_2} \qquad \text{I(15)}$$

which represents linear interpolation on the oscilloscope signals. This approximation leads to errors less than the experimental errors discussed in the text provided that the difference $T_{B2} - T_{B1}$ does not exceed about 200°K. For a typical experiment, using the chromium blue lines, suppose

$$T_{B2} = 2600°\text{K}$$
$$T_{B1} = 2400°\text{K}$$
$$T = 2500°\text{K (actual value).}$$

Substituting these values in I(13) and I(14) gives, as the ratio of the observed emission and absorption deflections

$$\frac{d_1}{d_2} = 0{\cdot}633.$$

If this value of d_1/d_2 is used in the linear interpolation formula I(15), then the evaluated temperature turns out to be 2478°K, which is lower than the true temperature by 22°K. If this first evaluation of T is substituted in I(14), an approximate value of β is found which may then be substituted in I(13) to give a better value of T. When this is carried out for the above example, the value of T turns out to be 2500°K and no further iterations are required. In the most accurate work, it is worth while carrying out this

iteration but as it was estimated that the accuracy of the temperature measurements in this work was not better than about $\pm 30°K$ and, in addition, non-uniformities are present in the gas sample, the simple direct linear interpolation given by I(15) was used to evaluate T and no iterations carried out.

If the photomultiplier responses in each beam are not the same for the same flux of radiation, then this will lead to an error in the value of T determined as described above. For photomultipliers having different responses, equations I(11) become

$$\begin{aligned} d_1 &= G_1 [B(\nu_0,T)-B(\nu_0,T_{B1})]\,\phi \\ d_2 &= G_2 [B(\nu_0,T_{B2})-B(\nu_0,T)]\,\phi \end{aligned} \qquad \text{I(16)}$$

These lead to the following relationship, similar to I(13):

$$T = T_{B1} + \frac{d_1}{d_1 + \frac{G_1}{G_2}\beta\, d_2}(T_{B2}-T_{B1}). \qquad \text{I(17)}$$

The photomultiplier sensitivities can be set equal to an accuracy of 10 per cent or better. Suppose that their responses differ by 10 per cent such that $G_1/G_2 = 0{\cdot}9$. Substituting this in I(17) and using the same values for the temperatures as above gives the actual value of d_1/d_2 to be 0·570. If now, the linear interpolation expression given in I(15) is used, the evaluated gas temperature, T, turns out to be 2473°K which differs from the linear interpolation result obtained assuming identical sensitivities by only 5°K. Thus, the sensitivities are not required to be identical to a high degree of accuracy.

The photomultiplier signals not only yield the temperature but may also be related to the relative concentration of the reversal atoms.

From equations I(11),

$$\phi = \int_{\Delta\nu_1} \xi_\nu \left[1-\exp\left\{ -\int_{-R}^{+R} \alpha_\nu(x)dx \right\} \right] d\nu = Q'(d_1+d_2) \qquad \text{I(18)}$$

where $Q' = G[B(\nu_0,T_{B2})-B(\nu_0,T_{B1})]$ and is constant for a given setting of the backing source temperatures. If it is now assumed that the absorption coefficient, $\alpha_\nu(x)$, remains constant across the tube and the transmission coefficient, ξ_ν, of the filter is constant over the bandwidth of the spectrum line, then I(18) becomes

$$\int_{\Delta\nu_1} (1-e^{-2\alpha_\nu R})d\nu = Q(d_1+d_2)$$

where Q is a constant.

Under the optically thick conditions of the experiment, it may be shown that the integral ('Total Absorption') varies as the square root of the reversal atom concentration[32]. Thus,

$$d_1+d_2 \propto N^{\frac{1}{2}}.$$

Thus, the relative change in reversal atom concentration during a shock tube run may be obtained from the sum of the absorption and emission signals.

APPENDIX II

Corrections made in Spectrum Line Reversal Temperature Measurements

The brightness temperature of the image of a backing source in the tube at the wavelength of the reversal line differs from the brightness temperature measured directly with an optical pyrometer because of light losses at lenses and windows and the variation of emissivity of tungsten with wavelength and temperature.

Notation

T_F	True filament temperature
S_{λ_1}	Brightness temperature of the backing source at wavelength λ_1 viewed directly through the envelope of the lamp
S'_{λ_1}	Brightness temperature at wavelength λ_1 of image of the backing source in shock tube
S_{λ_2}	Brightness temperature at wavelength λ_2 viewed directly
S'_{λ_2}	Brightness temperature at wavelength λ_2 of image in shock tube
ζ	Transmission coefficient of lenses and windows between the source and the image in the shock tube*
τ	Transmission coefficient of the glass envelope of a backing source*
$e(\lambda,T_F)$	Emissivity of the tungsten filament at wavelength λ and temperature T_F

The brightness temperature of the filament is measured, looking through the glass envelope of the lamp, using a disappearing filament pyrometer containing a red glass filter centred approximately on 6650Å (λ_1) but reversal is detected against the image of the source in the shock tube at the reversal wavelength λ_2. Therefore, the brightness temperature, S'_{λ_2}, of the image at wavelength λ_2, is to be determined from the pyrometer measurement, S_{λ_1}, and a knowledge of τ, ζ, and $e(\lambda,T_F)$.

Due to loss of light in the optical path,

$$B(S'_{\lambda_2}) = \zeta B(S_{\lambda_2}) \qquad \text{II(1)}$$

where B denotes the Planck function. Assuming that ζ does not vary with wavelength, we have also

$$B(S'_{\lambda_1}) = \zeta B(S_{\lambda_1}). \qquad \text{II(2)}$$

Eliminating ζ between II(1) and II(2) and using Wien's approximation to the Planck function, gives,

$$\frac{1}{S'_{\lambda_2}} = \frac{1}{S_{\lambda_2}} + \frac{\lambda_2}{\lambda_1}\left(\frac{1}{S'_{\lambda_1}} - \frac{1}{S_{\lambda_1}}\right). \qquad \text{II(3)}$$

Equation II(2) may also be written, after making Wien's approximation:

$$\frac{1}{S'_{\lambda_1}} - \frac{1}{S_{\lambda_1}} = -\frac{k\lambda_1}{hc}\log_e \zeta. \qquad \text{II(4)}$$

* It will be assumed that these transmission coefficients do not vary with wavelength.

The quantity $-\frac{k\lambda_1}{hc}\log_e \zeta$ on the right of II(4) is not dependent on temperature and is therefore constant for different temperatures.

Let
$$-\frac{k\lambda_1}{hc}\log_e \zeta = \beta \qquad \text{II(5)}$$

Substitution in II(3) then gives
$$\frac{1}{S'_{\lambda_2}} = \frac{1}{S_{\lambda_2}} + \frac{\lambda_2}{\lambda_1}\beta. \qquad \text{II(6)}$$

For a given optical arrangement, β can be determined by measuring several values of the brightness temperature directly (S_{λ_1}) and the corresponding brightness temperatures of the image (S'_{λ_1}). A plot of $1/S_{\lambda_1}$ against $1/S'_{\lambda_1}$ should then give a straight line from which β may be determined. A typical plot is shown in Fig. 24.

S_{λ_2}, the brightness temperature of the source viewed directly at the wavelength of the reversal line is determined from knowledge of the emissivity of tungsten as follows. The brightness temperature, S_λ, at some wavelength λ is related to the true filament temperature, T_F, by the relationship
$$B(S_\lambda) = \tau e(\lambda, T_F)\, B(T_F). \qquad \text{II(7)}$$

Using Wien's approximation, this becomes
$$\frac{1}{S_\lambda} = \frac{1}{T_F} - \frac{k\lambda}{hc}\log_e\{\tau e(\lambda, T_F)\}. \qquad \text{II(8)}$$

Therefore, assuming that τ does not vary with wavelength, we have for wavelengths λ_1 and λ_2 and given filament temperature T_F,
$$\frac{1}{S_{\lambda_1}} + \frac{k\lambda_1}{hc}\log_e\tau = \frac{1}{T_F} - \frac{k\lambda_1}{hc}\log_e e(\lambda_1, T_F) \qquad \text{II(9)}$$
$$\frac{1}{S_{\lambda_2}} + \frac{k\lambda_2}{hc}\log_e\tau = \frac{1}{T_F} - \frac{k\lambda_2}{hc}\log_e e(\lambda_2, T_F). \qquad \text{II(10)}$$

From published measurements of e as a function of λ and T_F, and a knowledge of τ, equations II(9) and II(10) may be used to prepare a curve relating S_{λ_1} and S_{λ_2}. The results of De Vos were used to prepare this curve[33]. The result for the blue wavelength of the chromium resonance lines is shown in Fig. 25. The relationship is seen to be linear. The dotted portion of the straight line is an extrapolation of this linear relationship to brightness temperatures higher than those explored by De Vos. The transmission coefficient of the glass envelope of a backing source was measured and found to be 0·870. This is found to make negligible difference to the relationship between S_{λ_1} and S_{λ_2} and may be neglected in using II(9) and II(10) to derive this relationship.

Some more recent results for the emissivity of tungsten have been obtained by Larrabee[34]. These do not extend to such a high temperature as De Vos' results but over the temperature range investigated by Larrabee, the relationship obtained between S_{λ_1} and S_{λ_2} is found to be very nearly the same as that obtained using De Vos' results. Certainly, within the accuracy of the temperature measurements given in this report, the difference between the two sets of emissivity results may be neglected.

Direct measurement with the pyrometer gives S_{λ_1}, from which S_{λ_2} may be determined from the relationship given in Fig. 25. This value of S_{λ_2} is then used in II(6) along with the pre-determined value of β to give S'_{λ_2} the brightness temperature of the source image at the wavelength of the reversal line. The corrections have to be made with care because they are not small. For example, from the curves given in Figs. 24 and 25 the correction to the temperature when the directly measured background temperature is 2500°K amounts to +70°K.

APPENDIX III

Boundary-Layer Transition to Turbulence

The transition to turbulence will depend on the Reynolds number based on the distance a particle travels to transition after being set in motion by the shock wave, the free-stream kinematic viscosity, and the velocity of the gas. The results for transition in various shock tubes have been collated by Hartunian, Russo and Marrone[35]. Although the results show fairly wide scatter, a transition Reynolds number of $1{\cdot}5 \times 10^6$ is fairly representative. Using this value of the transition Reynolds number, the curves of Fig. 21 were prepared, showing the distance from the end plate and the time after reflection at which the reflected shock wave is likely first to encounter a turbulent boundary layer. In view of the scatter of the results of Ref. 35 these curves must be regarded as tentative but at least they show that interaction with a turbulent boundary layer is likely to occur very soon after shock reflection.

APPENDIX IV

Idealised Wave Interactions in a Shock Tube and the preparation of Wave Diagrams

1. *General Remarks.*

Ideal shock tube theory was used to work out theoretical wave diagrams. The diaphragm is assumed to be removed instantaneously and effects of viscosity are neglected entirely. The contact surface is assumed to be a plane separating the driver and test gases and no mixing takes place across this plane.

The incident shock wave reflects from the closed end of the tube. When this reflected shock meets the contact surface, the nature of the interaction is determined by the conditions on either side of the contact surface.For some cases a shock wave will be reflected off the contact surface; for others an expansion wave will be reflected. For one particular value of the incident shock Mach number, which depends on the driver and test gases and on their relative temperatures, there will be no wave reflected from the contact surface and this will itself be brought to rest. This is known as the 'tailored' condition and, in theory, provides a shock-heated gas of steady conditions as soon as the incident shock wave is reflected from the end: this condition is obviously desirable for shock tunnel purposes. If the tailored mode is used, then the reservoir temperature is fixed for a given driver temperature. For example, when helium is used at room temperature (20°C), the tailoring shock Mach number is 3·4, giving a reflected shock temperature of 1574°K. This is rather low for high enthalpy studies. The temperature of the gas in the reflected shock region may be raised by two methods, using a given driver gas:

(1) The driver gas may be heated before bursting the diaphragm. This will raise the tailoring shock Mach number. This involves heating the barrel of the driver, a technique that has been used, for example, at Cornell Aeronautical Laboratory[6].

(2) The shock tube may be used in the overtailored condition; a shock wave is then reflected off the contact surface. In the overtailored condition, multiple reflections take place between the end wall and the contact surface but, theoretically, these waves rapidly become weak and the contact surface is ultimately brought to rest, giving steady conditions of temperature and pressure in the hot gas. The temperature is higher than that obtained at tailoring because a stronger incident shock is used and because the first reflection from the contact face is a shock which is stronger than ensuing reflections. It is this second method that has been explored in the present work.

The temperature results have shown poor agreement between theory and experiment after the reflected shock has interacted with the contact surface. The reasons for this have been discussed. Idealised wave diagrams have proved useful in so far as they have provided a theoretical framework in which to discuss

the results. The differences between measured temperatures and pressures and the theoretical values of these quantities give some indication of the magnitude of non-ideal shock tube phenomena that must be postulated to account for these differences.

2. *Reflection and Transmission of a Shock Wave at a Contact Surface.*

When the shock wave reflected from the closed end of the tube strikes the contact surface a shock wave is transmitted through the contact surface and a shock wave or expansion wave is reflected from the surface, depending on the ratio of internal energies of the gases on each side of the contact surface.

The condition for tailoring is given by:

$$\frac{\frac{\gamma_B+1}{\gamma_B-1}+\frac{p_{A2}}{p_{A3}}}{\frac{\gamma_{A2}+1}{\gamma_{A2}-1}+\frac{p_{A2}}{p_{A3}}}=\frac{m_{A2}(\gamma_{A2}-1)T_{B2}}{m_{B2}(\gamma_B-1)T_{A2}} \qquad \text{IV(1)}$$

where m is molecular weight, the remaining symbols have their usual meaning and the suffices denote values of quantities in the regions shown in Fig. 26. The right-hand-side of IV(1) is the ratio:

$$\frac{\text{Specific internal energy in region B}}{\text{Specific internal energy in region A}}$$

IV(1) is satisfied at only one value of the incident shock Mach number which turns out to be 3·4 for helium driving into nitrogen when the gases are initially at room temperature.

Referring to Fig. 27, consider the interaction of a shock wave with the contact surface after several reflections have taken place. Firstly, assume that this interaction is over-tailored and a shock wave is therefore reflected from the contact face. Conditions An and Bn are known and we wish to evaluate conditions $A(n+1)$, $A(n+2)$ and $B(n+2)$. This may be done by employing the following relationships:

$$\frac{U_{An}}{a_{An}}=-\frac{3-\gamma_{An}}{4}\cdot\frac{u_{An}}{a_{An}}+\sqrt{1+\left(\frac{\gamma_{An}+1}{4}\right)^2\cdot\left(\frac{u_{An}}{a_{An}}\right)^2} \qquad \text{IV(2)}$$

where a denotes sound speed

$$\frac{p_{A(n+1)}}{p_{An}}=\frac{2\gamma_{An}}{\gamma_{An}+1}\left(\frac{U_{An}}{a_{An}}+\frac{u_{An}}{a_{An}}\right)^2-\frac{\gamma_{An}-1}{\gamma_{An}+1} \qquad \text{IV(3)}$$

$$\left(\frac{a_{A(n+1)}}{a_{An}}\right)^2=\frac{T_{A(n+1)}}{T_{An}}=\frac{p_{A(n+1)}}{p_{An}}\cdot\frac{(\gamma_{An}+1)+(\gamma_{An}-1)\frac{p_{A(n+1)}}{p_{An}}}{(\gamma_{An}-1)+(\gamma_{An}+1)\frac{p_{A(n+1)}}{p_{An}}} \qquad \text{IV(4)}$$

The pressure ratio $\frac{p_{A(n+2)}}{p_{A(n+1)}}$ across the shock after reflection from the contact surface has been given, for example, in Ref. 36. This pressure ratio is given by the equation:

$$\frac{A}{\sqrt{P'+B}}+\frac{1}{\sqrt{P'+\alpha_{An}}}-\frac{AP'}{\sqrt{P'+B}}\cdot\frac{p_{An}}{p_{A(n+1)}}-\frac{P'}{\sqrt{P'+\alpha_{An}}}-k\sqrt{P'}=0 \qquad \text{IV(5)}$$

where

$$\frac{1}{P'} = \frac{p_{A(n+2)}}{p_{A(n+1)}}$$

$$A = \sqrt{\frac{En}{h} \cdot \frac{p_{A(n+1)}}{p_{An}}}$$

$$B = \frac{\gamma_B + 1}{\gamma_B - 1} \cdot \frac{p_{A(n+1)}}{p_{An}}$$

$$En = \frac{m_A(\gamma_{An} - 1)\, T_{Bn}}{m_B(\gamma_B - 1)\, T_{An}}$$

$$h = \frac{\dfrac{\gamma_{An}+1}{\gamma_{An}-1} \cdot \dfrac{p_{An}}{p_{A(n+1)}} + 1}{\dfrac{\gamma_{An}+1}{\gamma_{An}-1} + \dfrac{p_{An}}{p_{A(n+1)}}}$$

$$k = \frac{1 - \dfrac{p_{An}}{p_{A(n+1)}}}{\sqrt{\dfrac{\gamma_{An}+1}{\gamma_{An}-1} \cdot \dfrac{p_{An}}{p_{A(n+1)}} + 1}}, \qquad \alpha = \frac{\gamma+1}{\gamma-1}.$$

Equation IV(5) is readily solved by Newton's method. When $\frac{p_{A(n+2)}}{p_{A(n+1)}}$ has been determined from IV(5), this quantity may then be used to find remaining quantities appropriate to region $A(n+2)$ by means of the following equations:

$$\frac{U_{A(n+1)}}{a_{A(n+1)}} = \left\{ \frac{\gamma_{A(n+1)} - 1}{2\gamma_{A(n+1)}} + \frac{\gamma_{A(n+1)} + 1}{2\gamma_{A(n+1)}} \cdot \frac{p_{A(n+2)}}{p_{A(n+1)}} \right\}^{\frac{1}{2}} \qquad \text{IV(6)}$$

$$\left(\frac{a_{A(n+2)}}{a_{A(n+1)}} \right)^2 = \frac{T_{A(n+2)}}{T_{A(n+1)}} = \frac{p_{A(n+2)}}{p_{A(n+1)}} \cdot \frac{(\gamma_{A(n+1)} + 1) + (\gamma_{A(n+1)} - 1)\dfrac{p_{A(n+2)}}{p_{A(n+1)}}}{(\gamma_{A(n+1)} - 1) + (\gamma_{A(n+1)} + 1)\dfrac{p_{A(n+2)}}{p_{A(n+1)}}} \qquad \text{IV(7)}$$

$$\frac{u_{A(n+2)}}{a_{A(n+2)}} = \frac{\dfrac{p_{A(n+2)}}{p_{A(n+1)}} - 1}{\sqrt{\gamma_{A(n+2)}(\gamma_{A(n+2)} - 1)\left(\dfrac{p_{A(n+2)}}{p_{A(n+1)}}\right)^2 + \gamma_{A(n+2)}(\gamma_{A(n+2)} + 1)\dfrac{p_{A(n+2)}}{p_{A(n+1)}}}} \qquad \text{IV(8)}$$

$$\frac{p_{B(n+2)}}{p_{Bn}} = \frac{p_{A(n+2)}}{p_{A(n+1)}} \cdot \frac{p_{A(n+1)}}{p_{An}} \qquad \text{IV(9)}$$

$$\frac{U_{Bn}}{a_{Bn}} = \sqrt{\frac{\gamma_B - 1}{2\gamma_B} + \frac{\gamma_B + 1}{2\gamma_B} \cdot \frac{p_{B(n+2)}}{p_{Bn}}} - \frac{u_{An}}{a_{Bn}} \qquad \text{IV(10)}$$

The speed of the tail of the expansion wave is then given by

$$V_{A(n+1)} = u_{A(n+2)} + a_{A(n+2)}. \qquad \text{IV(16)}$$

Equations IV(9) to IV(11) are then used to give U_{Bn}, $a_{B(n+2)}$ and $T_{B(n+2)}$.

Quantities appropriate to region $A(n+3)$ are given by:

$$\frac{a_{A(n+3)}}{a_{A(n+1)}} = \frac{2a_{A(n+2)}}{a_{A(n+1)}} - 1 \qquad \text{IV(17)}$$

$$\frac{T_{A(n+3)}}{T_{A(n+1)}} = \left(\frac{a_{A(n+3)}}{a_{A(n+1)}}\right)^2 \qquad \text{IV(18)}$$

$$\frac{p_{A(n+3)}}{p_{A(n+1)}}^{\frac{\gamma_{A(n+2)}-1}{2\gamma_{A(n+2)}}} = 2\left(\frac{p_{A(n+2)}}{p_{A(n+1)}}\right)^{\frac{\gamma_{A(n+2)}-1}{2\gamma_{A(n+2)}}} - 1. \qquad \text{IV(19)}$$

The speed of the head of expansion reflected from the closed end of the shock tube is given by

$$U_{A(n+2)} = -u_{A(n+2)} + a_{A(n+2)}. \qquad \text{IV(20)}$$

The speed of the tail of the reflected expansion wave is given by

$$V_{A(n+2)} = a_{A(n+3)}. \qquad \text{IV(21)}$$

Depending on the ratio of internal energies across the contact surface, a compression or a rarefaction will be reflected from the contact surface when the expansion wave meets it.

In cases of interest to this paper it is found that a compression is reflected. The pressure ratio across this is given by [37]

$$w(1-x) + (w+y-1-yzx^{BB})\sqrt{\frac{\alpha_{A(n+2)}x+1}{\beta_{A(n+2)}}} = 0 \qquad \text{IV(22)}$$

where

$$x = \frac{p_{A(n+4)}}{p_{A(n+3)}}$$

$$w = \left(\frac{p_{A(n+3)}}{p_{A(n+2)}}\right)^{\beta_{A(n+2)}}$$

$$\beta = \frac{\gamma-1}{2\gamma}$$

$$z = \left(\frac{p_{A(n+3)}}{p_{A(n+2)}}\right)^{\beta_B}$$

$$y = \left(\frac{\beta_{A(n+2)}}{\beta_B} E_{(n+2)}\right)^{\frac{1}{2}}.$$

Equation IV(22) may be solved by Newton's method. The ratios $\frac{T_{A(n+4)}}{T_{A(n+5)}}$ and $\frac{u_{A(n+4)}}{a_{A(n+4)}}$ may be evaluated by using equations of the same form as IV(7) and IV(8), employing appropriate values in the right-hand-side.

The speed of the head of the compression reflected from the contact surface is given by

$$u_{A(n+3)} = a_{A(n+3)} \qquad \text{IV(23)}$$

and the speed of the tail by

$$V_{A(n+3)} = a_{A(n+4)} + u_{A(n+4)}. \qquad \text{IV(24)}$$

$U_{A(n+4)}$ and the conditions behind the compression reflected from the closed end of the tube are then given by equations of the same form as IV(2) to IV(4).

An expansion wave is transmitted through the contact surface. The following relationships hold:

$$\frac{T_{B(n+4)}}{T_{B(n+2)}} = \left(\frac{p_{A(n+4)}}{p_{A(n+2)}}\right)^{2\beta_B} \qquad \text{IV(25)}$$

$$U_{B(n+2)} = a_{B(n+2)} - u_{A(n+2)} \qquad \text{IV(26)}$$

$$V_{B(n+2)} = a_{B(n+4)} - u_{A(n+4)}. \qquad \text{IV(27)}$$

The above procedure may then be repeated for the next interaction. In practice, since the initial shock Mach number is less than 3·4, the subsequent waves are very weak and it is only necessary to evaluate conditions as far as A7 (*see* Fig. 26) which means that only the first two interactions with the contact surface need be considered.

The calculations for both the under-tailored and over-tailored case were carried out on the N.P.L. ACE computer for $M_s = 1{\cdot}2(0{\cdot}2)3{\cdot}2$ and $M_s = 3{\cdot}6(0{\cdot}2)5{\cdot}6$. For the under-tailored case the interactions as far as region A7 of Fig. 26 were evaluated. For the over-tailored case the interactions as far as region A16 were evaluated. The input data were obtained from Bernstein's theoretical results for conditions behind the incident and reflected shock in nitrogen[9]. Real gas effects were partly taken into account by evaluating γ, the ratio of specific heats, behind each wave. This was done by fitting a polynomial expression up to the second power of the temperature to the results given in Ref. 38.

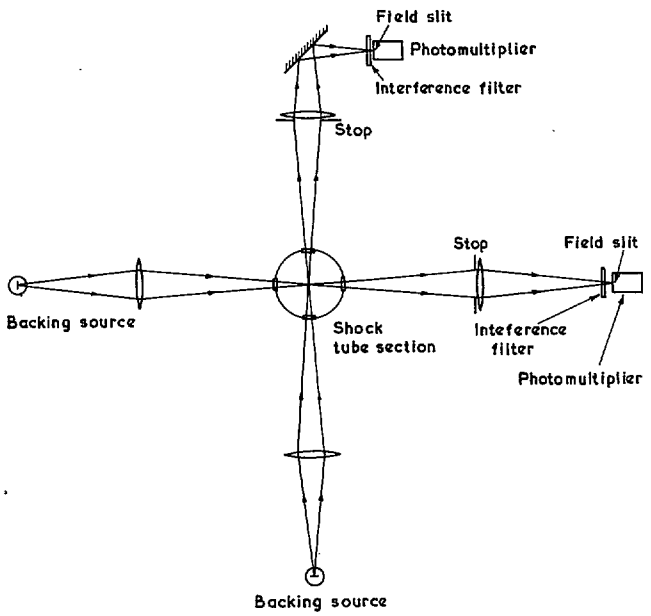

FIG. 1. Double beam arrangement with mutually perpendicular beams (not to scale).

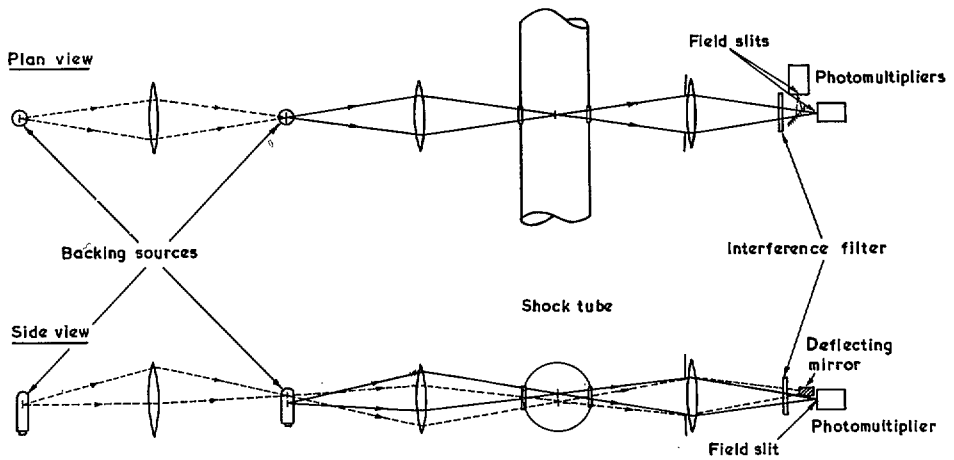

FIG. 2. Double beam arrangement with beams lying close together (not to scale).

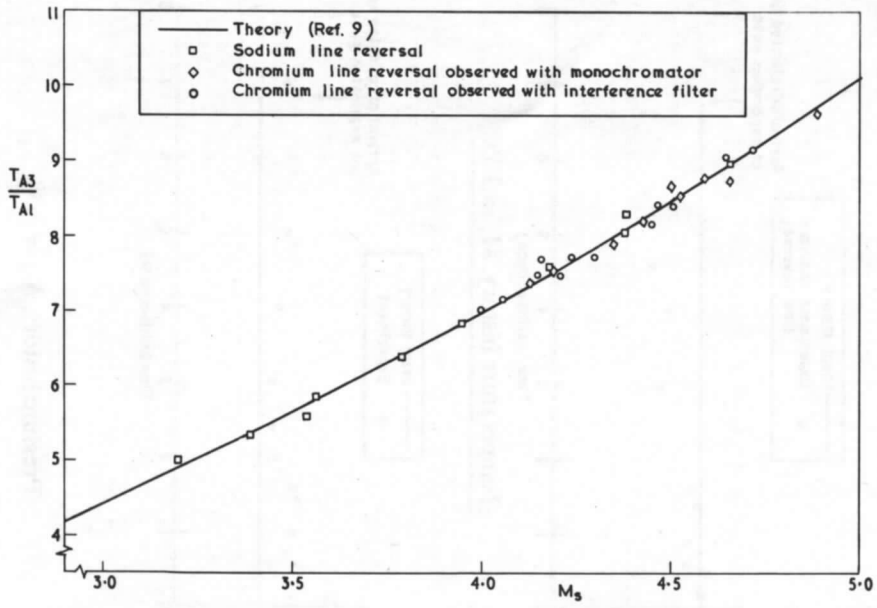

FIG. 3. Temperature behind reflected shock wave.

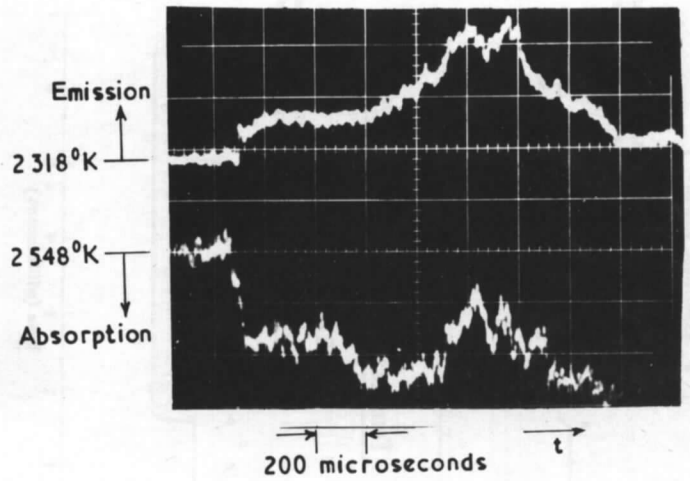

FIG. 4. Double-beam temperature record using chromium blue resconance lines. $M_s = 4{\cdot}45$.

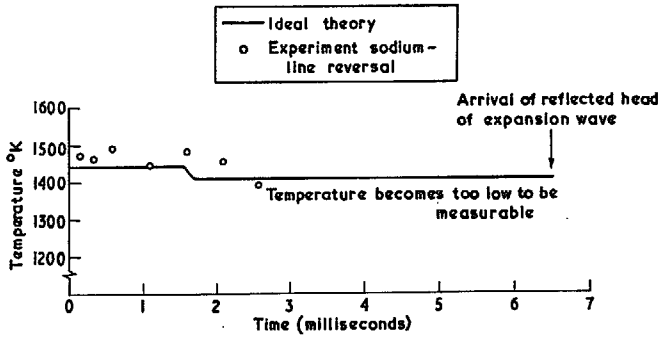

Temperature history, $M_s = 3{\cdot}20$.

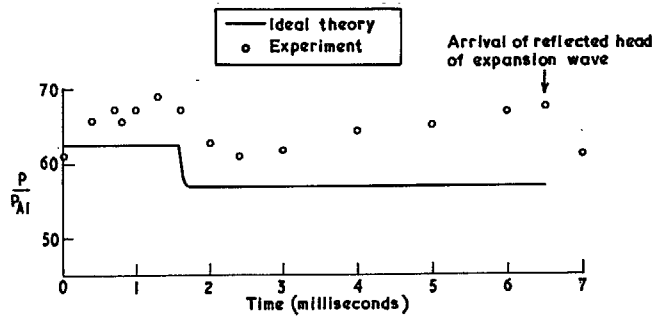

Pressure history, $M_s = 3{\cdot}20$.

FIG. 5.

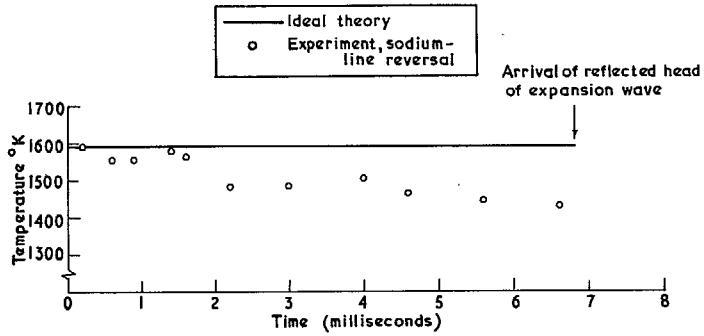

Temperature history, $M_s = 3{\cdot}39$.

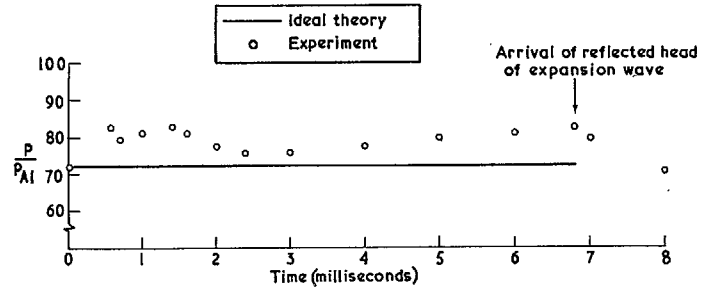

Pressure history, $M_s = 3{\cdot}38$.

FIG. 6.

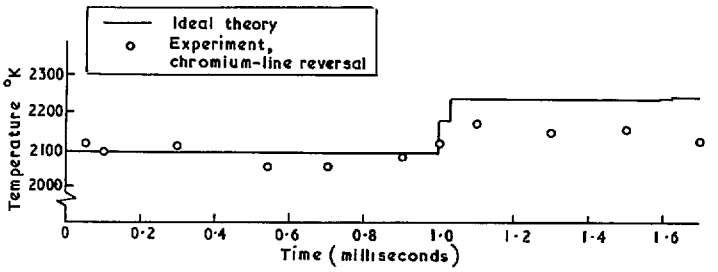

Temperature history, $M_s = 4{\cdot}06$.

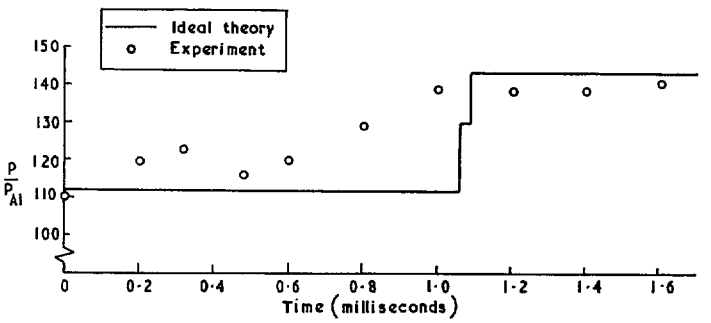

Pressure history, $M_s = 3{\cdot}96$.

FIG. 7.

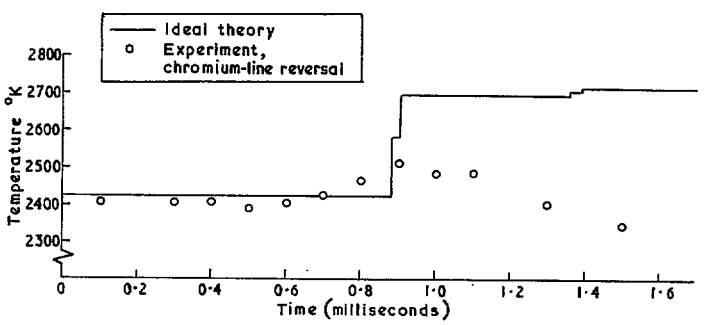

Temperature history, $M_s = 4{\cdot}45$.

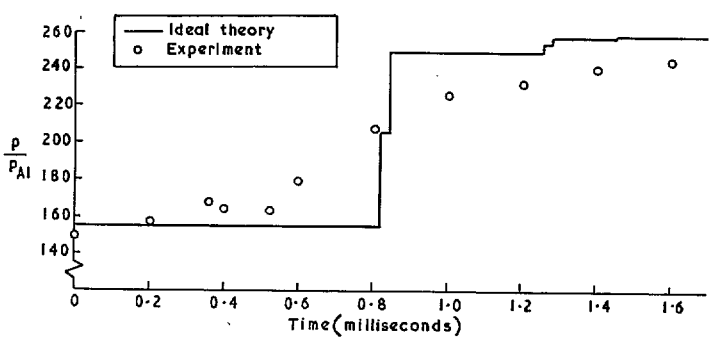

Pressure history, $M_s = 4{\cdot}48$.

FIG. 8.

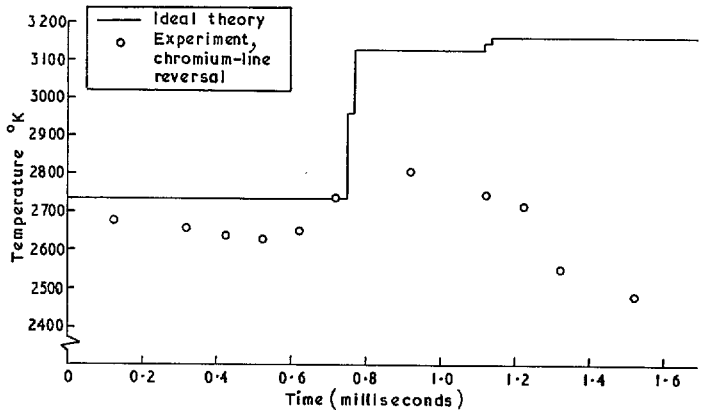

Temperature history, $M_s = 4{\cdot}75$.

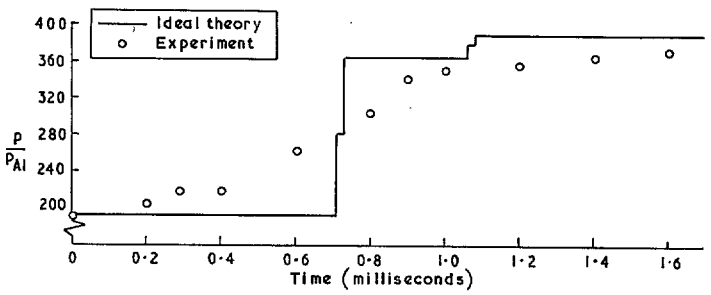

Pressure history, $M_s = 4{\cdot}87$.

FIG. 9.

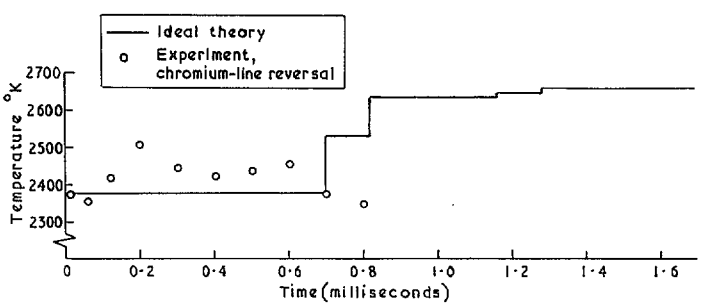

FIG. 10. Temperature history, $M_s = 4{\cdot}41$. Observations made 2·5 in. from closed end of tube.

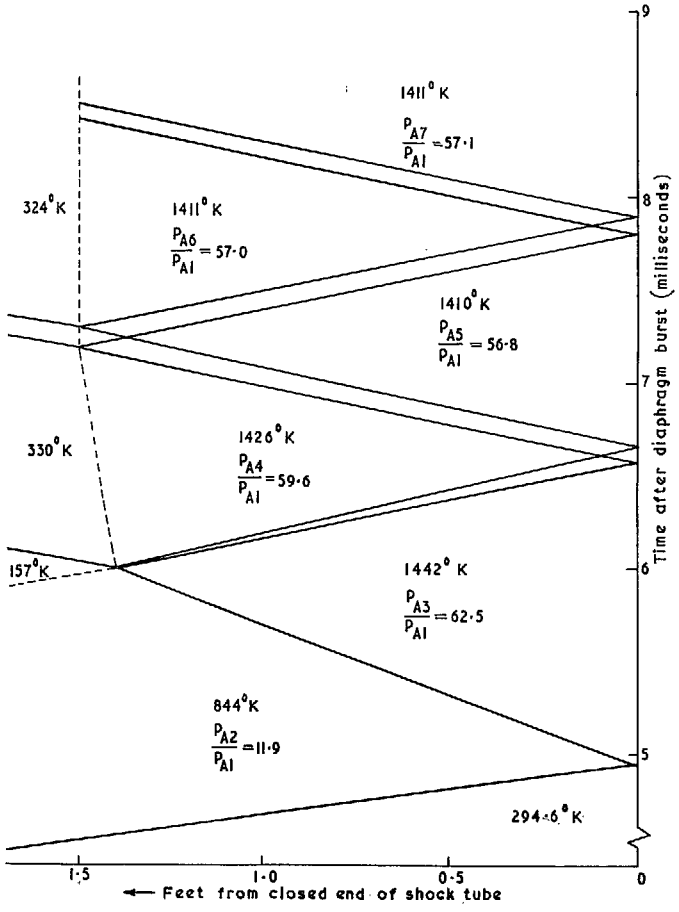

FIG. 11. Wave diagram, $M_s = 3{\cdot}20$.

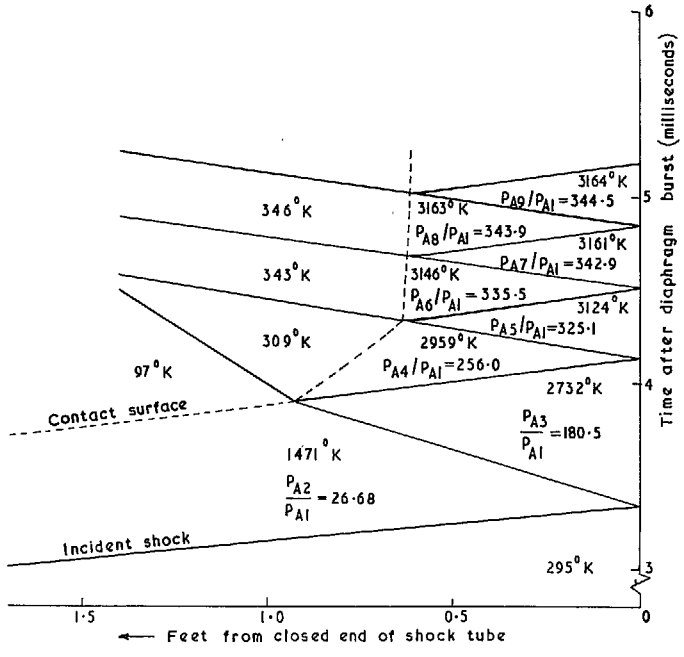

FIG. 12. Wave diagram, $M_s = 4{\cdot}75$.

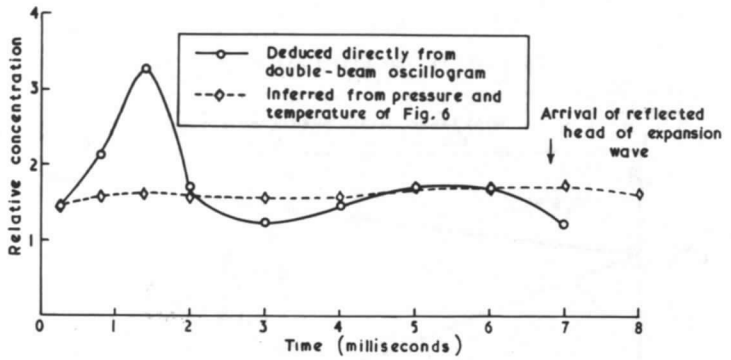

FIG. 13. Relative concentration of sodium atoms, $M_s = 3{\cdot}39$.

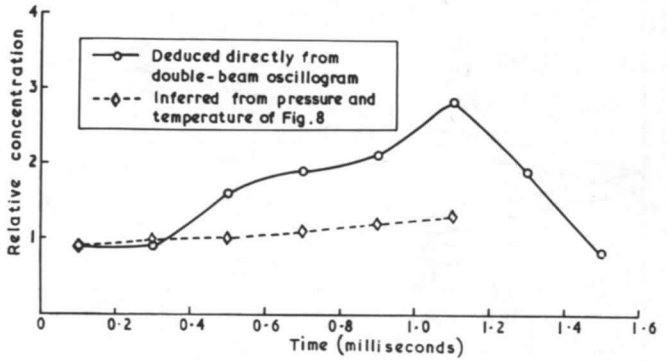

FIG. 14. Relative concentration of chromium atoms, $M_s = 4{\cdot}45$.

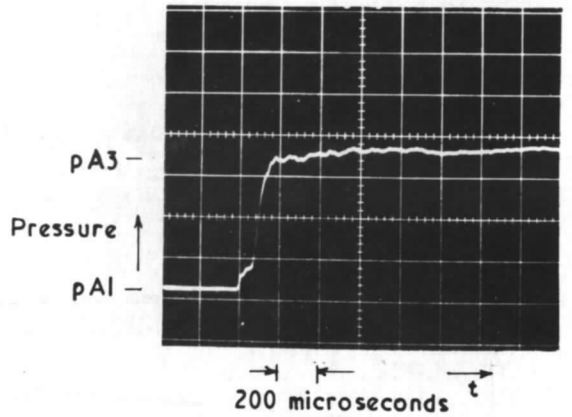

FIG. 15. Pressure records at $M_s = 3{\cdot}20$.

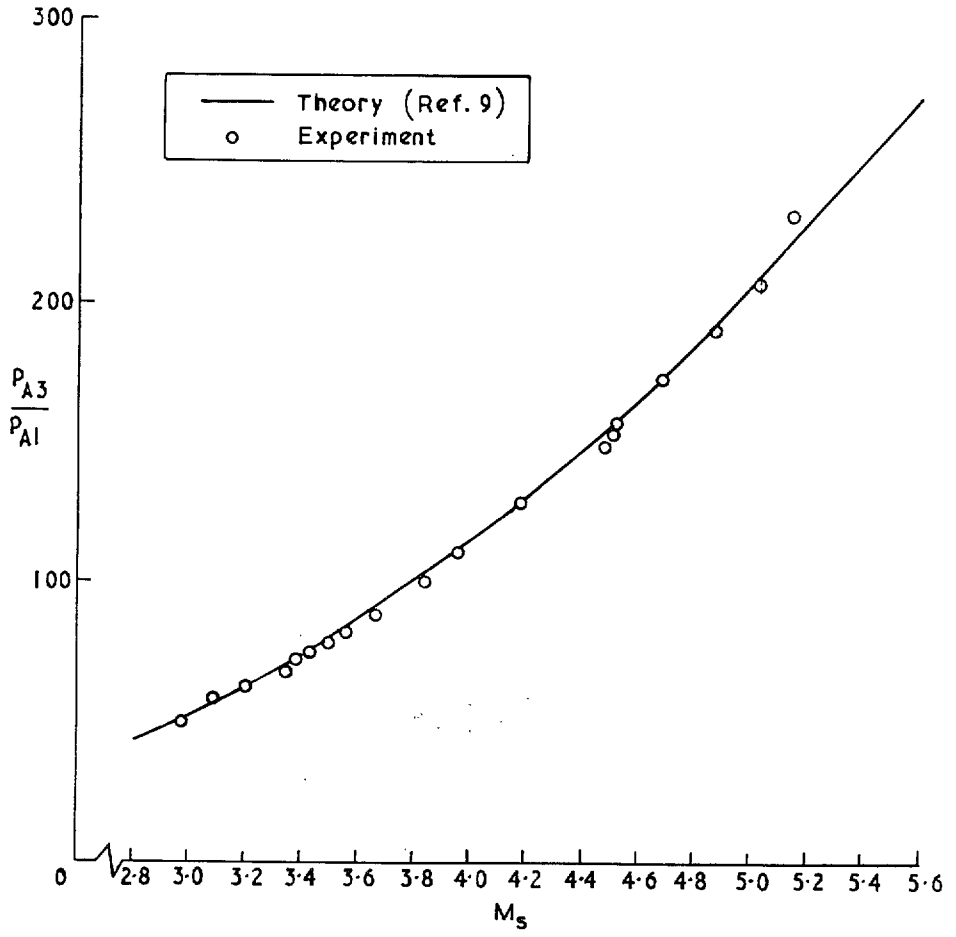

FIG. 16. Pressure behind reflected shock wave.

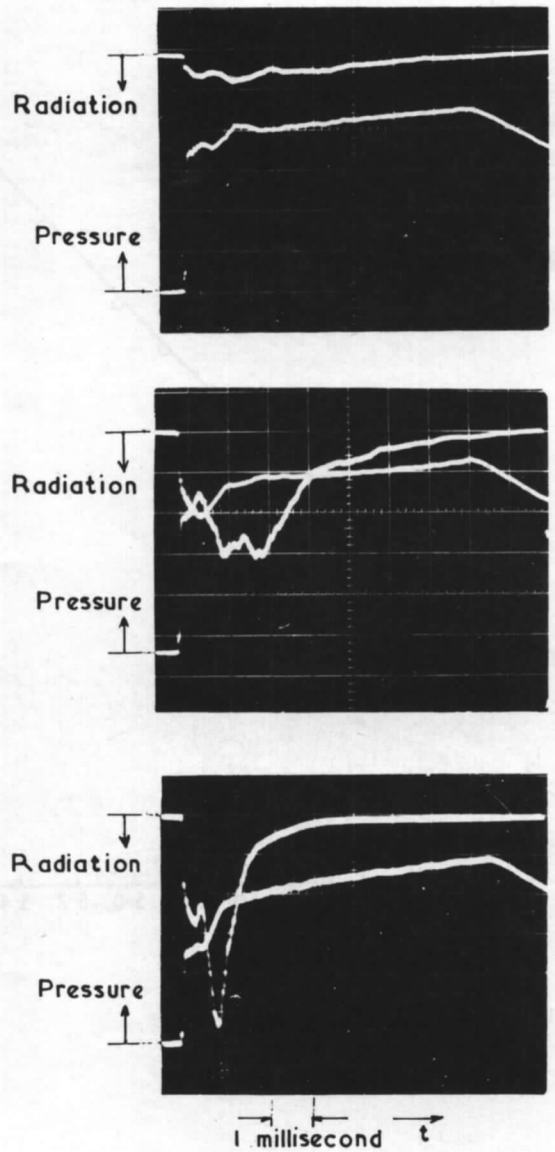

FIG. 17
$M_s = 3.66$

FIG. 18
$M_s = 3.96$

FIG. 19
$M_s = 4.52$

FIG . 17 to 19. Comparison of duration of high pressure and duration of high temperature at different values of M_s.

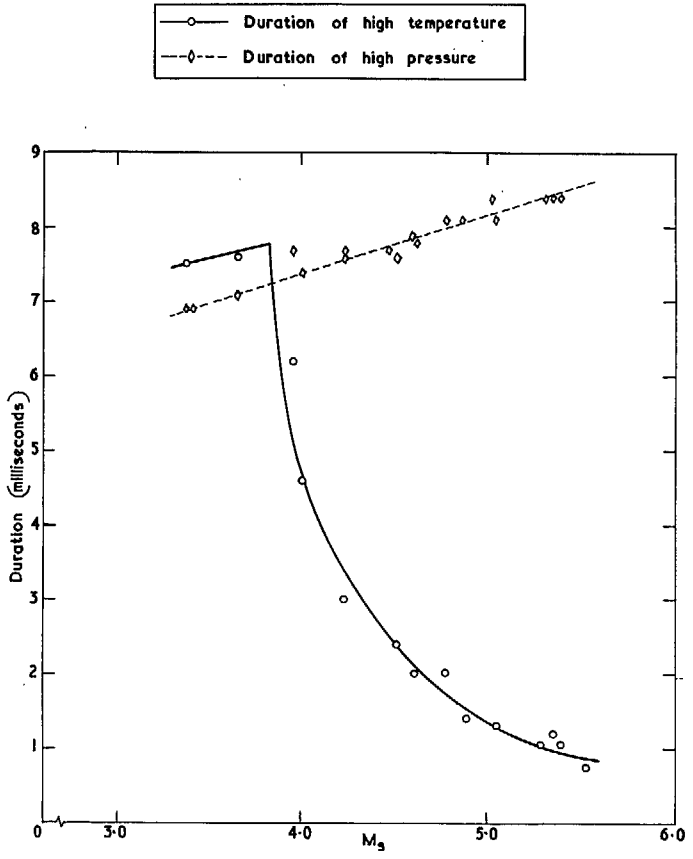
Duration of high temperature
Duration of high pressure
Duration (milliseconds)
0
1
2
3
4
5
6
7
8
9
3·0
4·0
5·0
6·0
M_s

FIG. 20.

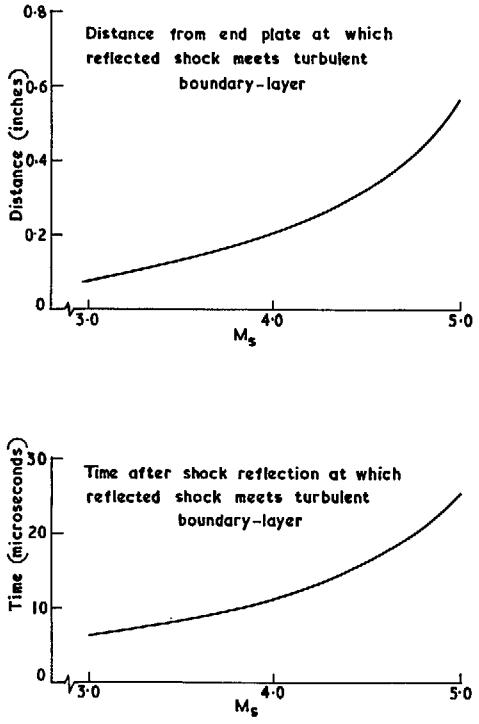
Distance from end plate at which reflected shock meets turbulent boundary-layer
Distance (inches)
0
0·2
0·4
0·6
0·8
3·0
4·0
5·0
M_s
Time after shock reflection at which reflected shock meets turbulent boundary-layer
Time (microseconds)
0
10
20
30
3·0
4·0
5·0
M_s

FIG. 21.

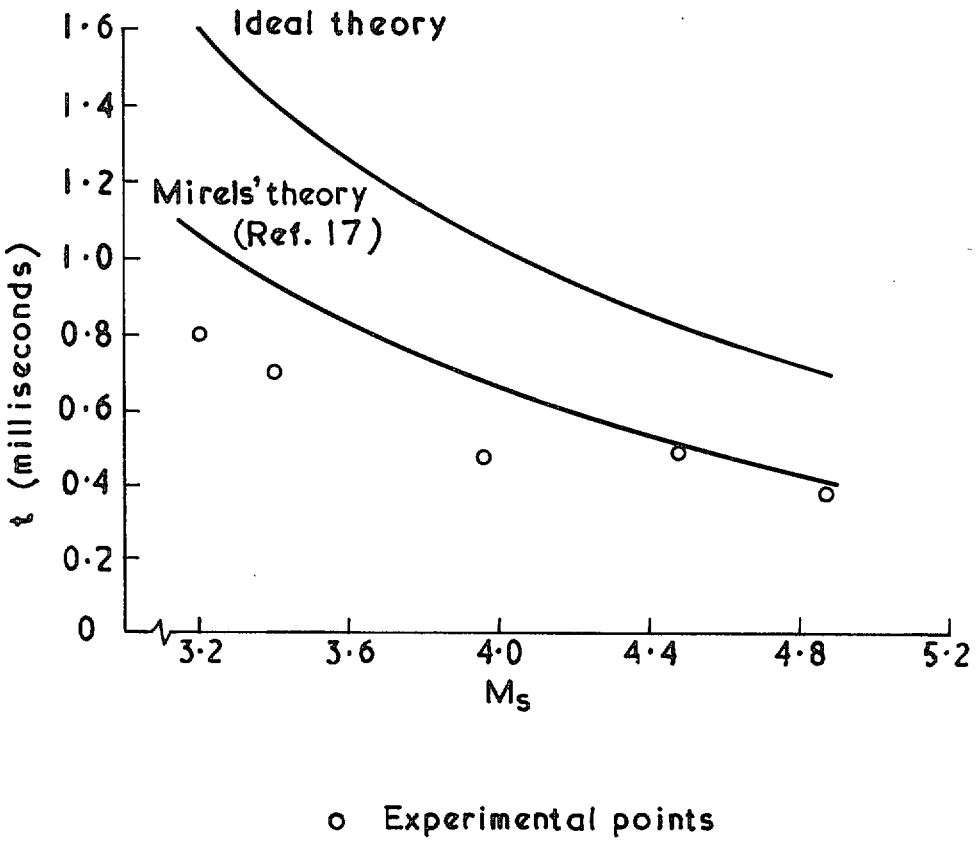

FIG. 22. The time of arrival at the end of the tube of the disturbance reflected off the contact region.

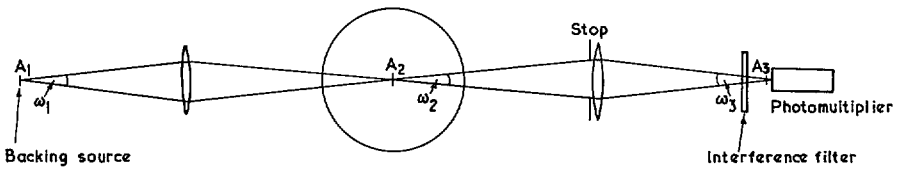

FIG. 23. A_1 and A_2 are conjugate images of A_3, the area of the slit in front of the photomultiplier.

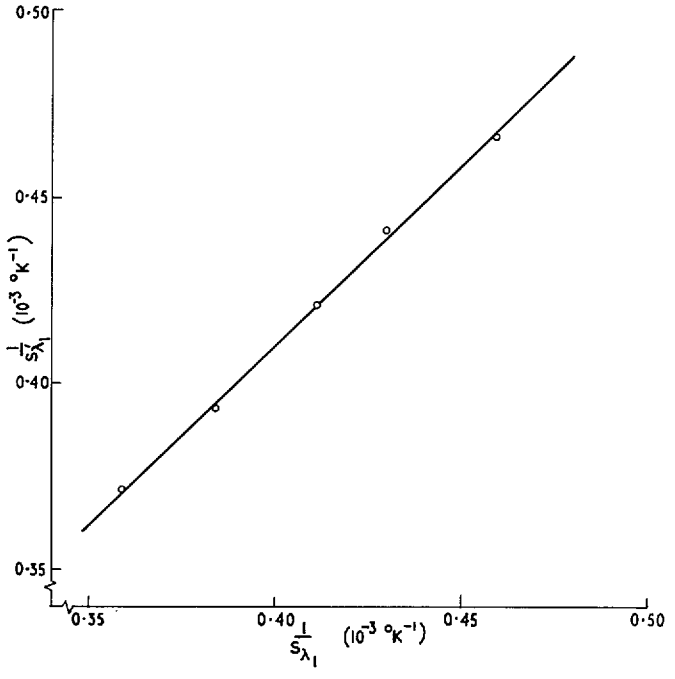

FIG. 24. Linear relationship between $1/S_{\lambda_1}$ and $1/S'_{\lambda}$.

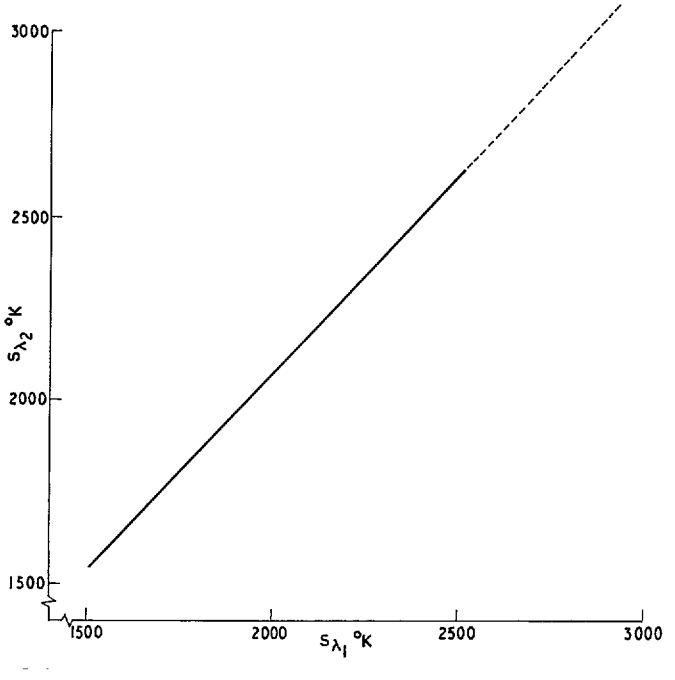

FIG. 25. Relationship between S_{λ_1} and S_{λ_2} using emissivity data of De Vos and $\lambda_1 = 6650$Å, $\lambda_2 = 4275$Å.

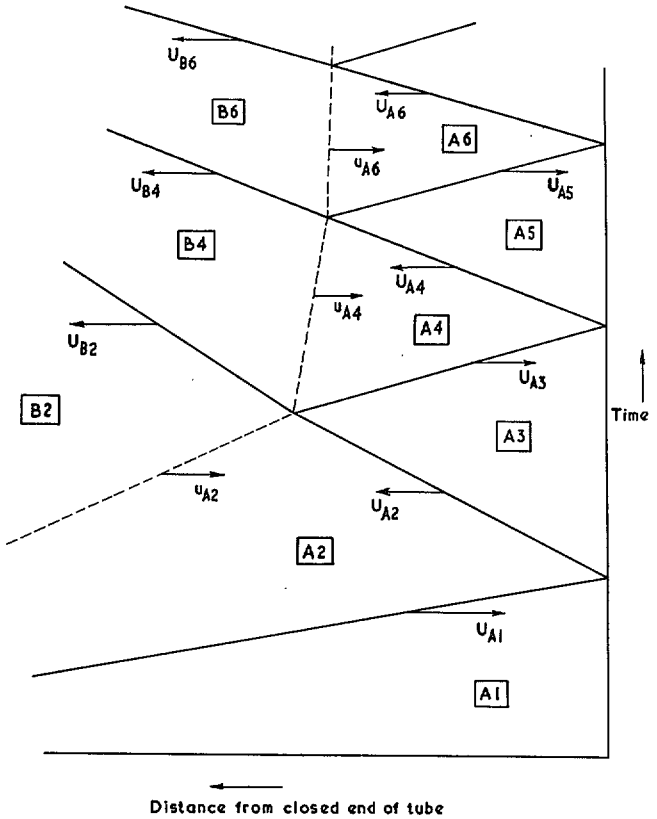

FIG. 26. Notation for wave processes.

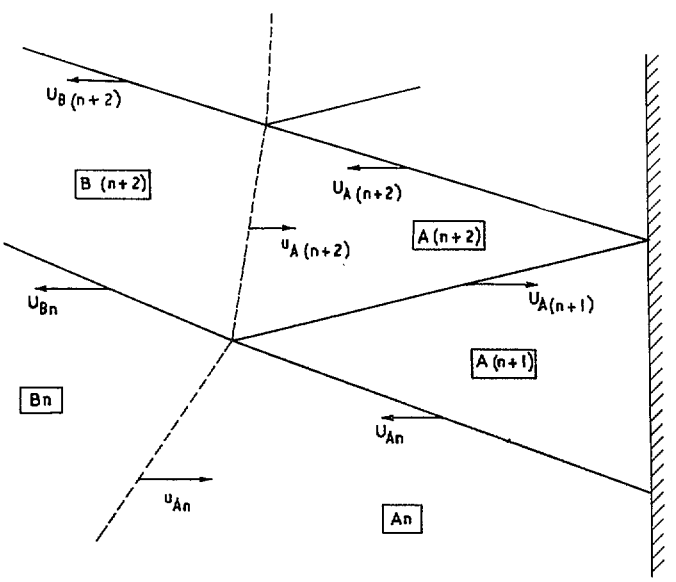

FIG. 27. Interaction of shock with contact surface. Overtailored case.

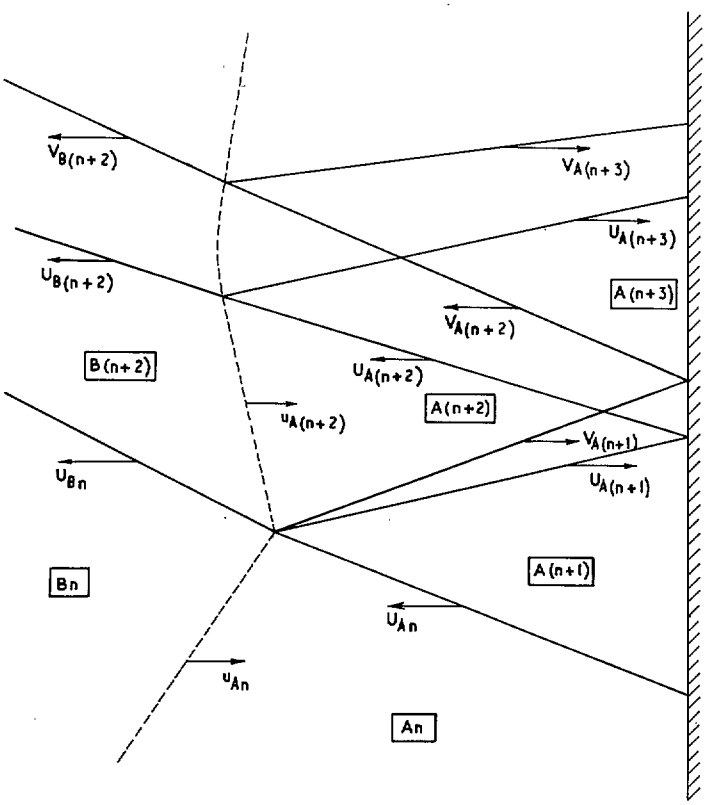

FIG. 28. Interaction of shock with contact surface. Undertailored case.

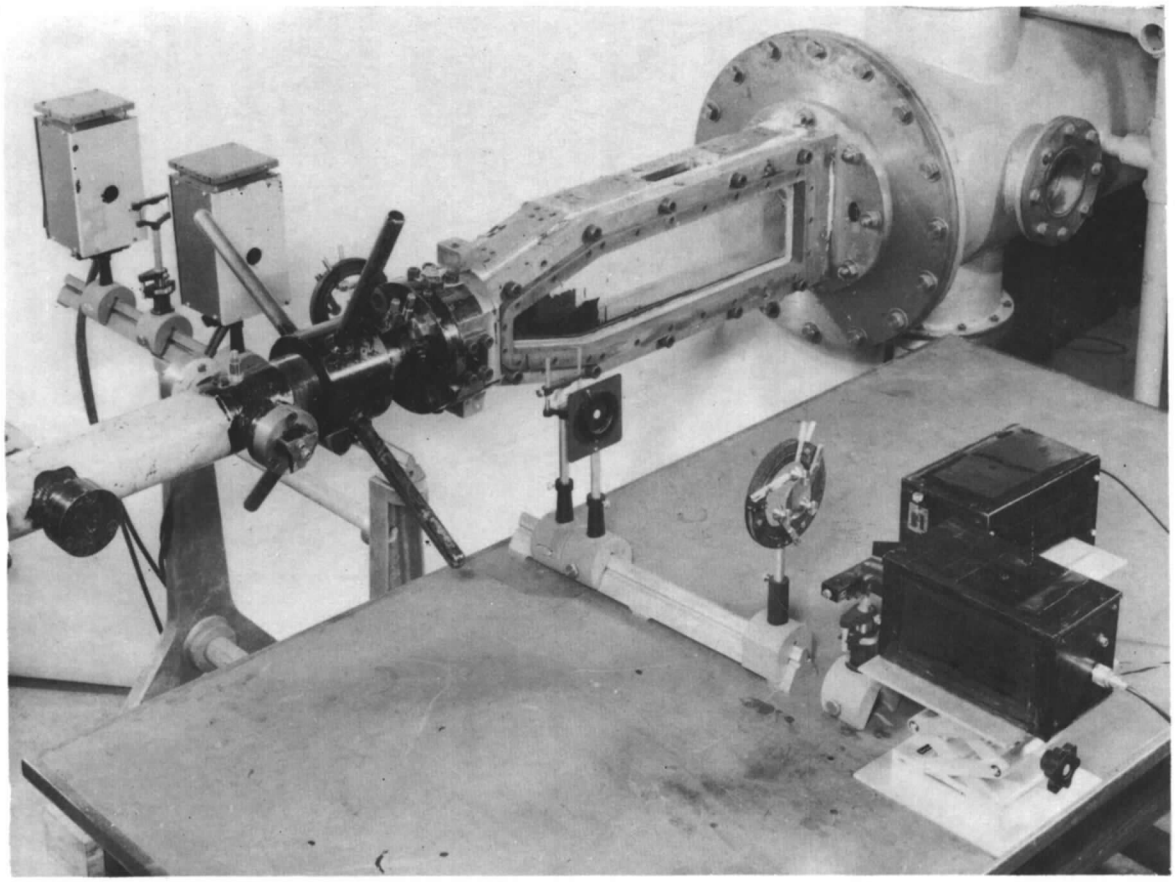

PLATE I. Double-beam apparatus for reversal temperature measurements.

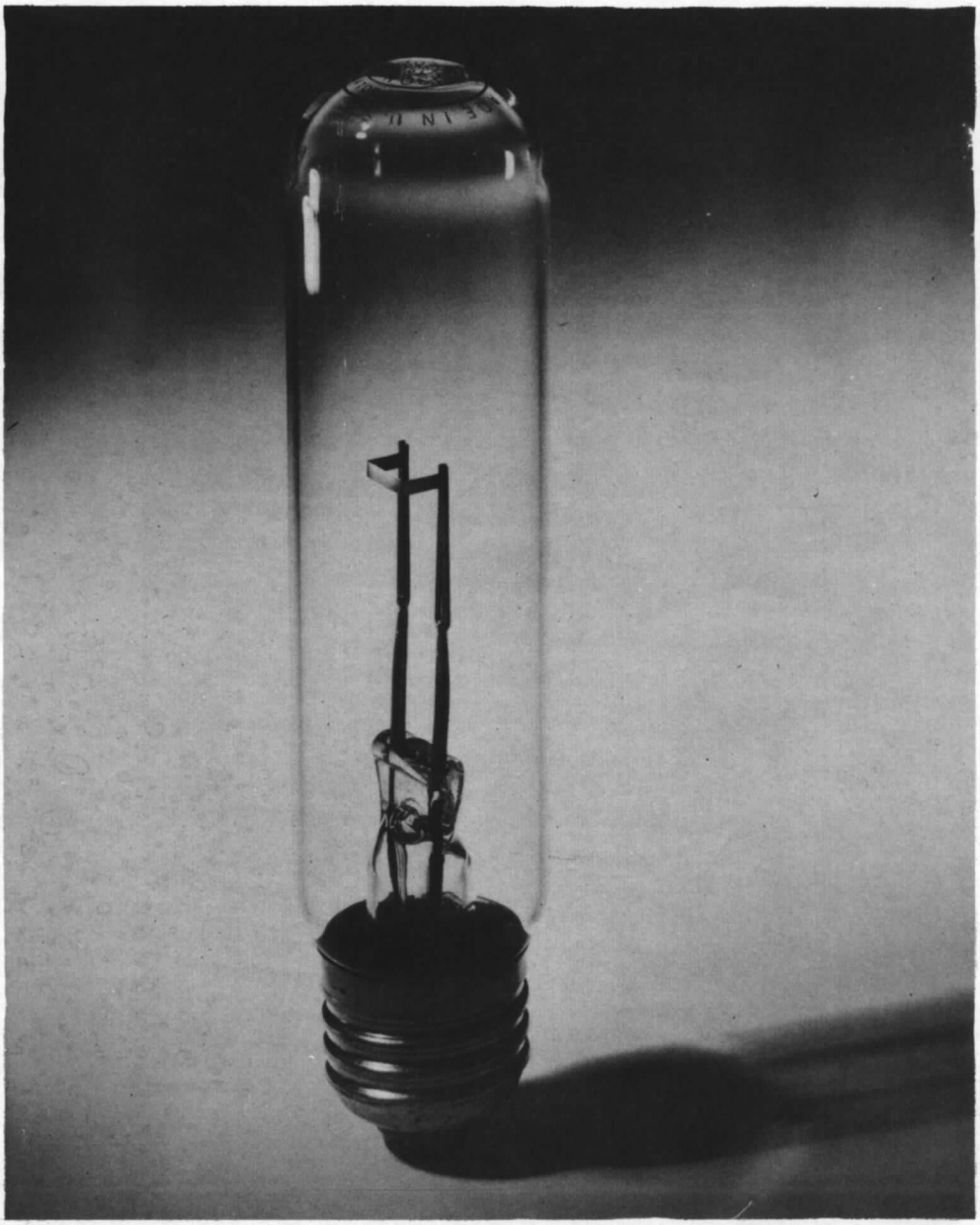

PLATE II. Microscope illuminator used for backing source in reversal temperature measurements.

Printed in Wales for Her Majesty's Stationery Office by Allens (Cardiff) Limited

Dd.125874 K4

Published by
HER MAJESTY'S STATIONERY OFFICE

To be purchased from
49 High Holborn, London W.C.1
423 Oxford Street, London W.1
13A Castle Street, Edinburgh 2
109 St. Mary Street, Cardiff
Brazennose Street, Manchester 2
50 Fairfax Street, Bristol 1
35 Smallbrook, Ringway, Birmingham 5
7–11 Linenhall Street, Belfast 2
or through any bookseller

S.O. Code No. 23–3479